Marine and Petroleum Geology 158 (2023) 106506

Contents lists available at ScienceDirect

Marine and Petroleum Geology

journal homepage: www.elsevier.com/locate/marpetgeo

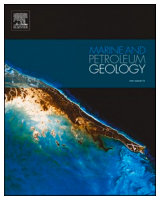

The effect of chlorite rims on reservoir quality in Chang 7 sandstone reservoirs in the Ordos Basin, China

Wenchao Dou [a], Mian Lin [a,b,*], Luofu Liu [c,d], Langbo Jia [e]

[a] Key Laboratory for Mechanics in Fluid Solid Coupling Systems, Institute of Mechanics, Chinese Academy of Sciences, Beijing, 100190, China
[b] University of Chinese Academy of Sciences, Beijing, 100190, China
[c] State Key Laboratory of Petroleum Resources and Prospecting, China University of Petroleum (Beijing), Beijing 102249, China
[d] Basin and Reservoir Research Center, College of Geosciences, China University of Petroleum (Beijing), Beijing 102249, China
[e] Exploration and Development Research Institute of Petro-China Changqing Oil Field Company Ltd, Xi'an Shaanxi 710018, China

ARTICLE INFO

Keywords:
Sandstone reservoir
Porosity preservation
Chlorite rim
Diagenesis

ABSTRACT

Chlorite rims have been of interest to petroleum geologists over the past several decades, as a significant number of abnormal high-porosity sandstone reservoirs at great depths have been related to chlorite rims. To clarify the contribution of chlorite rims to porosity preservation in sandstones, the relationship between chlorite rims and porosity evolution in Chang 7 sandstones of the Upper Triassic Yanchang Formation in the Ordos Basin in north-central China was investigated using thin sections, scanning electron microscopy, energy dispersive X-ray spectroscopy, and X-ray diffraction analyses. Based on the detrital composition and diagenetic evolution pathway analyses, it was concluded that chlorite rims inhibited the formation of quartz cementation. However, in addition to quartz cementation, compaction and other cements (commonly carbonates and clays) also control the porosity evolution of sandstones. In sandstones in which porosity reduction is largely controlled by compaction or other cements, chlorite rims may have a limited effect on porosity preservation. Thus, chlorite rims can play an important role in porosity preservation only in sandstones in which quartz cementation is the main process of porosity destruction. The results of this study indicate that the development of high-porosity sandstones is often controlled by many factors, and the effects of chlorite rims on porosity preservation are not always significant.

1. Introduction

The porosity of sandstone generally decreases with increasing burial depth. However, as listed in Table 1, a large number of deeply buried sandstone reservoirs worldwide with anomalously high porosity have been reported in recent decades. Several major causes of this phenomenon have been identified in previous studies, including: (1) anomalously low temperatures (Taylor et al., 2010); (2) grain coats and rims, including clays and microcrystalline quartz (Bloch et al., 2002); (3) early emplacement of hydrocarbons (Marchand et al., 2000, 2001, 2002; Worden et al., 1998; 2018); and (4) fluid overpressure at shallow depths (Scherer, 1987; Ramm and Bjørlykke, 1994).

Grain coats and rims are known as one of the most important porosity preservation mechanisms. Chlorite rims are probably the most common grain rims that have been found to have a close relationship with many deeply buried highly porous sandstones (Ehrenberg, 1993; Hillier S, 1994; Bloch et al., 2002; Ajdukiewicz et al., 2010). Due to this, they are of increasing interest to geologists, and are the focus of this study. Previous studies have suggested that chlorite rims may contribute to preserving porosity by inhibiting quartz cementation (Ehrenberg, 1993; Hillier, 1994; Pittman and Lumsden, 1968). Sandstones with chlorite rims generally have relatively high porosity compared to sandstones with no clay rims at similar depths and with similar burial-temperature histories. Detailed reviews of chlorite rims and their effects on reservoir quality have been previously reported by Dowey et al. (2012) and Worden et al. (2020). A compilation of several published typical case studies of chlorite rims is presented in Tables 1 and in which the sandstones listed are all deeply buried hydrocarbon reservoirs that are rich in chlorite rims, which are usually considered to be one of the most important factors contributing to porosity preservation. However, it is obvious that in these sandstone reservoirs, chlorite rims are generally not the only factor responsible for porosity preservation. Other

* Corresponding author. Key Laboratory for Mechanics in Fluid Solid Coupling Systems, Institute of Mechanics, Chinese Academy of Sciences, Beijing, 100190, China.
E-mail address: linmian@imech.ac.cn (M. Lin).

https://doi.org/10.1016/j.marpetgeo.2023.106506
Received 28 March 2023; Received in revised form 14 September 2023; Accepted 15 September 2023
Available online 25 September 2023

factors, such as relative high-energy sandstones, anomalously low temperatures, early emplacement of hydrocarbons and fluid overpressure at shallow depths, may also contribute to porosity preservation. On this basis, it is necessary to reevaluate the contribution of chlorite rims to porosity preservation.

Chang 7 sandstones in this study are one of the typical chlorite-rich sandstones, and are selected as the study area. According to previous studies (Chen et al., 2014; Li et al., 2021; Zhang et al., 2011, 2012), some relatively high porosity sandstones in Ordos Basin are thought to be related to chlorite rims. The aims of this study were to 1) investigate the importance of chlorite rims for porosity preservation and 2) determine the factors that control the contribution of chlorite rims to porosity preservation.

2. Geological settings

The Ordos Basin is the second largest sedimentary basin in China and is located in north-central China. The entire basin can be divided into six major structural units (Editorial Committee of Petroleum Geology of Changqing Oilfield, 1992): the Weibei uplift, the Yimeng uplift, the western edge thrust belt, the Jinxi fold belt, the Tianhuan sag, and the Yishan slope (Fig. 1).

The Upper Triassic Yanchang Formation is deposited in a lacustrine delta sedimentary system (Yang et al., 2005). The Yanchang Formation contains 10 members from the base to the top: Chang 10–Chang 1 (Fig. 2a) (Yao et al., 2009). When Chang 7 member was deposited, the lake expanding evolution reached its peak stage (Guo et al., 2014; Li et al., 2018). Subsequently, with the delta sedimentation gradually extending towards the center of the basin, the lake basin gradually shrank during the deposition period of Chang 6 (Guo et al., 2014; Li et al., 2018). At the time that Chang 6–7 was deposited, the basin was primarily filled with NE–SW-trending delta sedimentary systems, between which widespread gravity-flow deposits were deposited in the NW–SE-trending deep water area (Fig. 2b). As a result, Chang 6 and Chang 7 members consist of thick organic-rich shales and interbedded sandstones, acting as both excellent source rocks and reservoirs (Yang and Zhang, 2005; Li et al., 2009). These sandstones were mainly deposited in gravity flows, distributary channels, and mouth bar environments, while the shales were mainly deposited in interdistributary channels or were of lacustrine origin (Zou et al., 2010; Yang et al., 2017).

The burial and thermal evolution history of a well in the study area are shown in Fig. 3. At the end of the Early Cretaceous, the Yanchang Formation achieved its maximum burial depth (approximately 2500 m) during the entire burial stage (Ren, 1996; Ren et al., 2007, 2008). Subsequently, the Ordos Basin was subjected to continuous uplift and erosion until loess was deposited in the Quaternary (Ren, 1996; Shi et al., 2012).

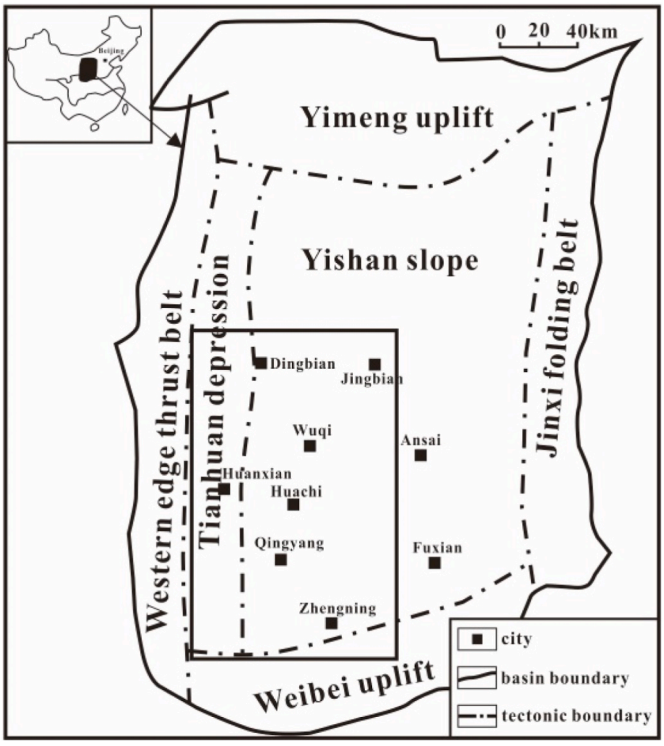

Fig. 1. Simplified structural map of the Ordos Basin.

3. Samples and methods

In total, 29 sandstone samples from Chang 7 member intervals from 15 wells in the Ordos Basin were collected for this study. All the wells in the study area have similar burial-temperature histories (shown in Fig. 3), in which the studied sandstones were mainly deposited in gravity flows and delta front environment. Thin sections impregnated

Table 1
A summary of porosity preservation causes in sandstones rich in chlorite rims. It is obvious that in these sandstone reservoirs, chlorite rims are generally not the only factor responsible for porosity preservation. Here, relative high-energy sandstones represent sandstones that are deposited in high-energy hydrodynamic environment, they are relative coarse-grained and contain less ductile components such as detrital matrix and clays.

Location		Middle Sichuan Basin	Kela-Keshen area, Tarim Basin	Santos Basin	Middle Indus Basin	Gulf of Mexico
Target reservoir(s)		Upper Triassic sandstones	Lower Cretaceous sandstones	Upper Cretaceous sandstones	Cretaceous volcaniclastic sandstones	Miocene sandstones
Sedimentary environment		fluvial-lacustrine	fluvial-lacustrine	turbidite and shallow-marine	shallow-marine	offshore deep-water
Maximum depth during burial period/m		4000–5000	6500–7000	~4500	3000–3500	~5500
Maximum temperature during burial period/°C		~150	~180	~125	~175	~130
Causes of porosity preservation	Relative high-energy sandstones	✓	✓	✓	✓	✓
	Anomalously low temperature					✓
	Fluid overpressure at shallow depths	✓	✓			✓
	Early emplacement of hydrocarbons			✓		
	Grain coats and rims	✓	✓	✓	✓	✓
Sources		Liu et al., 2016; Cai (2019)	Lai et al. (2017); Guo et al. (2016)	Bahlis and De Ros (2013)	Berger et al. (2009)	Taylor et al. (2010); Lander and Walderhaug, 1999

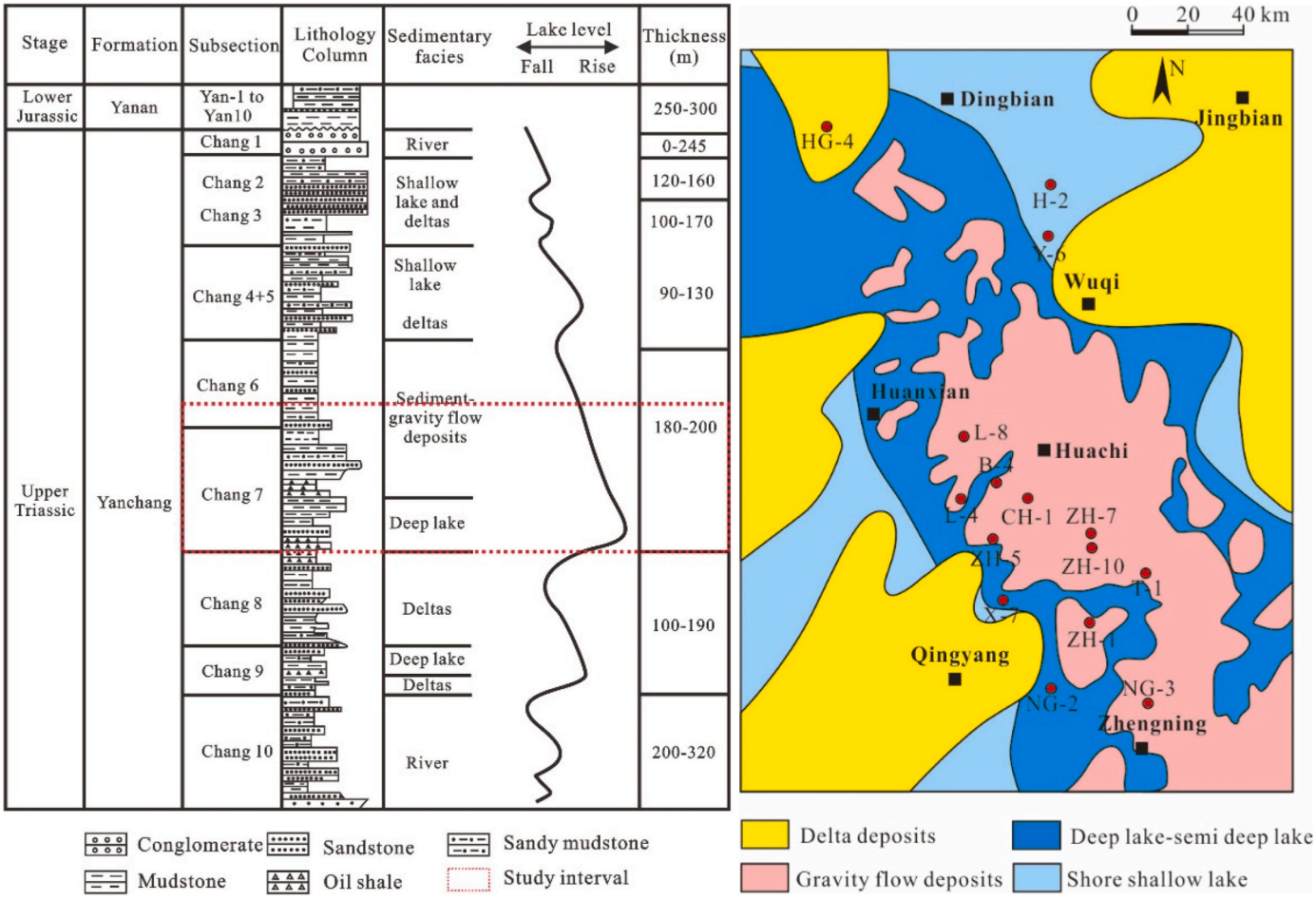

Fig. 2. (a) Triassic succession of the Ordos Basin showing Upper Triassic strata, lithology, lake basin evolution, sedimentary facies (modified after Guo et al., 2014; Li et al., 2018). (b) Distribution of the lake-delta system during Chang 6–7 periods of the Yanchang Formation (modified after Li et al., 2018).

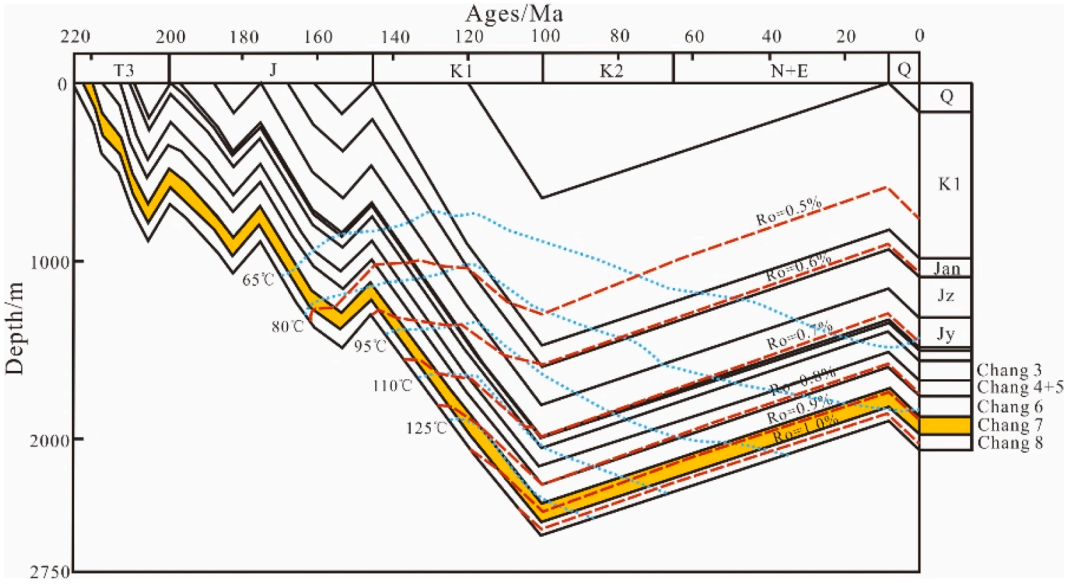

Fig. 3. Burial and thermal evolution history of well *X*41 in the study area (modified after Guo et al., 2013).

with blue epoxy were examined using a petrographic microscope. Half of each thin section was stained with Alizarin Red S- and K-ferricyanide for carbonate mineral determination. Quantitative petrographic analysis was performed by counting at least 300 points/thin sections, to differentiate between detrital composition, cements, and types of pores. Moreover, the grain size distribution was petrographically determined by measuring the long axis of 200 grains/thin section. In this study, the grain coat coverage was quantified by determining the ratio of the

surface perimeter of coated grains to the total surface perimeter (coated and uncoated). The measurement of grain coat coverage was only performed for quartz grains. When calculating the total surface perimeter, surfaces were excluded if they were in contact with other detrital component. The surface perimeter was determined using CorelDRAW *X7* software. The measurement of grain coat coverage was performed on 10 randomly selected images (1.26 mm × 0.95 mm) for each thin section.

Scanning electron microscope analysis (secondary electron (SE) and backscattered electron (BSE) modes) was performed on gold-coated, freshly broken rock chips and polished thin sections using an FEI Quanta 200 F scanning electron microscope equipped with an EDAX Genesis 2000 energy dispersive X-ray spectroscopy (EDS) system. The purpose of these analyses was to determine the size, morphology and paragenesis of the different authigenic minerals (particularly clay minerals) and to confirm the mineral identification results via EDS analysis.

Powdered samples were prepared using a combination of a grinding mill and an agate mortar. Clay fractions smaller than 2 μm were obtained by centrifuging the suspension. The oriented X-ray diffraction (XRD) samples were prepared by pipetting the clay suspensions onto glass slides. The mineralogical compositions of the clays were determined by XRD using a Bruker D2 phaser at 40 kV and 100 mA over a scanning range of 0°–30°2θ, a rate of 1 s/step, and a step size of 0.02°2θ. Each sample was analyzed by XRD after air drying, saturation with ethylene glycol, and heating to 550 °C.

The core plugs (2.5 cm in diameter) were chemically cleaned using a Soxhlet extraction apparatus and vacuum-oven dried in preparation for routine core analysis. Helium porosimeter (UltraPore-300) was used for porosity measurement following Boyle's law, and air-permeability instrument (UltraPerm-400) was used for Klinkenberg permeability analysis based on steady-state gas flow measurement with confining pressure at approximately 200 psi.

4. Results

4.1. Lithofacies

Based on observations of cores, six lithofacies are distinguished of the Chang 7 sandstone reservoirs. Fig. 4 shows detailed core descriptions of two typical Wells.

(i) Lithofacies 1

Lithofacies 1 is composed of fine-to medium-grained sandstones with parallel bedding (Fig. 5a), cross-bedding or ripple bedding (Fig. 5b). These sandstones are usually thick (generally 2–10 m), and are typically normally graded. It mainly develops in the margin of lake basin.

(ii) Lithofacies 2

Lithofacies 2 generally consists of fine-grained sandstones to siltstones. This lithofacies typically is reversely graded and very rare in the

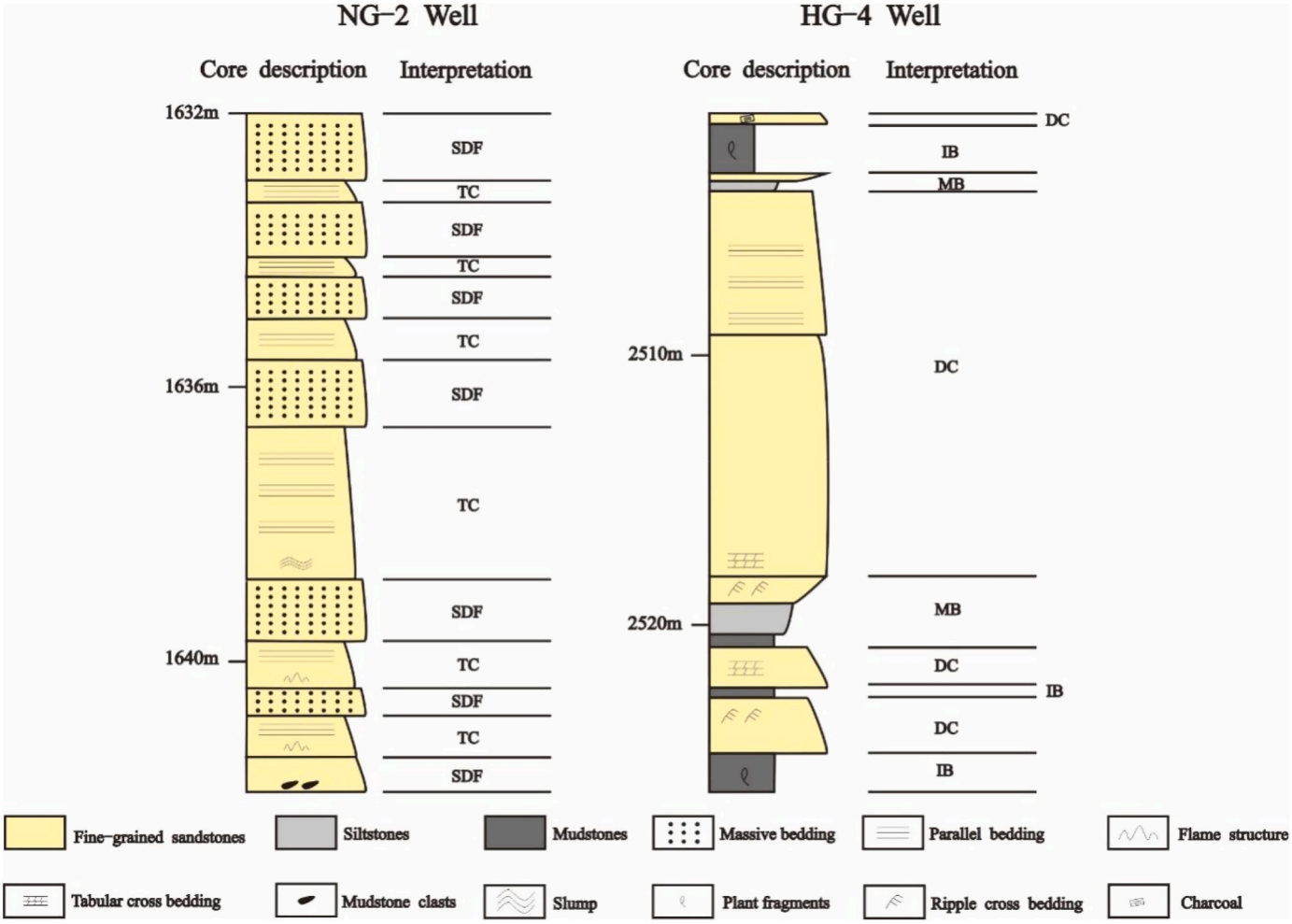

Fig. 4. Sedimentological characteristics of typical wells, with core description and interpretation of depositional environment. DC = distributary channels; IB = interdistributary bays; MB = mouth bars; SDF = sandy debris flow; TC = turbidity current.

Fig. 5. Sedimentological characteristics of cores in the Chang 7 sandstones. a) Parallel bedding, L-8, 2295.25 m; b) ripple bedding, H-2, 2146.35 m; c) load structures, NG-3, 1671.4 m; d) convolute bedding, NG-3, 1694.9 m; e) slump deformation, ZH-5, 2012.7 m; f) massive sandstones, L-4, 1913.32 m.

study area.

(iii) Lithofacies 3

Lithofacies 3 (usually <2 m) generally consists of siltstones to mudstones, containing rare plant stem fossils. This lithofacies is commonly intimately associated with Lithofacies 1.

(v) Lithofacies 4

Lithofacies 4 is composed of fine-grained sandstone, siltstone, and mudstone. Sandstones display various bedding characteristics, including parallel, ripple, and horizontal bedding. In addition, numerous deformation structures such as load structures (Fig. 5c), convolute bedding (Fig. 5d), and slump structures (Fig. 5e) are developed. This lithofacies is widely distributed in the study area, and mainly develops in the center of lake basin.

(iv) Lithofacies 5

Lithofacies 5 is composed of fine-grained, massive sandstones (Fig. 5f). It is widely distributed in the study area, and commonly intimately associated with Lithofacies 4.

(vi) Lithofacies 6

Lithofacies 6 is composed of thick (generally >2 m) dark mudstones. It is widely distributed in the study area, sometimes containing rare fish fossils.

4.2. Detrital composition

The Chang 7 sandstones are predominantly moderate to moderately well sorted, subangular to subrounded, and very fine-to fine-grained. Most sandstones are lithic arkoses, feldspathic litharenites, and litharenites, according to the classification scheme of Folk (1968), with an average framework composition of $Q_{51}F_{18}L_{31}$ (Fig. 6). The detrital quartz generally has an average content of 1.4%. Plagioclase usually has a higher content than K-feldspar. The total feldspar content is 5.1% in average. Rock fragments (average 1.4%) in decreasing order are granitoid (interlocked quartz-feldspar), metamorphites (quartz-mica schist) and sedimentary fragments (chert, silt or mud fragments).

The observed ductile components include detrital mica, detrital matrix (finer materials in sediments, typically includes detrital clay minerals), and ductile lithic fragments, such as phyllite, slate, and schist. Heavy minerals, including garnet, sphene, zircon, and tourmaline, are generally rare. The detailed results of the thin-section analysis are summarized in Table 2.

4.3. Pore types

Three main types of pores were identified by thin-section analysis: intergranular pores, intragranular pores, and oversized pores.

Primary intergranular pores essentially retain originally depositional intergranular spaces; they are regularly triangular or polygonal in shape (Fig. 7a). However, most intergranular pores are modified by subsequent cementation or dissolution, which often results in irregular pore margins. Strictly speaking, these modified intergranular pores are of hybrid primary-secondary origin in most cases but, for simplicity, all of them are regarded as primary pores in this study.

Intragranular pores mainly result from dissolution of the grain interiors such as feldspars and lithic fragments (especially volcanic lithic fragments) (Fig. 7b). Oversized pores (Fig. 7c) resulting from the intense dissolution of sedimentary material were occasionally observed. In this study, the secondary pores included both intragranular and oversized pores. Because some of these secondary pores may be filled with cement, the amount of grain dissolution should be equal to the sum of secondary

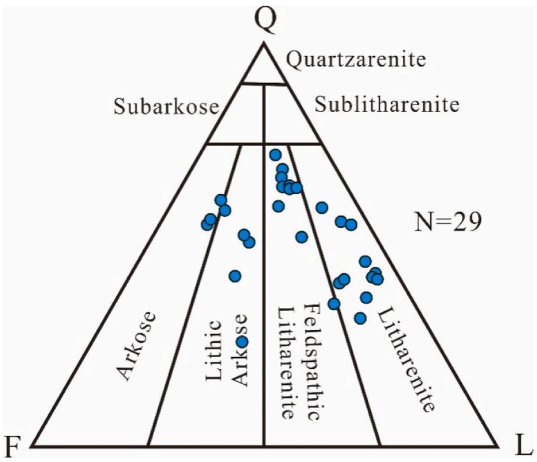

Fig. 6. QFL classification of the Chang 7 sandstones (after Folk, 1968).

Table 2

Petrologic and petrophysical parameters of the Chang 7 sandstones. The porosity and permeability data are from routine core analyses. Q = Quartz; F = Feldspar; L = Lithic fragments; RL = Rigid lithic fragments; DL = Ductile lithic fragments; Mi = Mica, including mainly biotite and less muscovite; HM = Heavy minerals such as garnet, sphene, zircon and tourmaline.; Ma = Matrix; CC = Carbonate cements; QC = Quartz cement; PLC= Pore-lining clays; PFC = Pore-filling clays; TSP = Thin-section porosity; Mz = Mean grain size; So = Trask sorting; DC = Ductile components (=DL + Mi + Ma); GD = Grain dissolution (= Intra TSP + Intra CC + Intra PFC); GCC = Grain coat coverage; DCS = distributary channels; IB = interdistributary bays; MB = mouth bars; SDF = sandy debris flow; TC = turbidity current; OP = Original porosity (=20.9 + 22.90/So, after Beard and Weyl (1973)). OP refers to sandstones porosity immediately after deposition and after minor compactional arrangement; COPL= Compactional porosity loss (COPL = OP - $\frac{(100 \times IGV) - (OP \times IGV)}{(100 - IGV)}$), after Ehrenberg (1989)); Pre-PLC = Pre-pore-lining clays porosity, its value equals to the sum of intergranular porosity and the volume of cements that fill intergranular pore-space (= Inter TSP + QC + Inter CC + Inter PFC + PLC); Pre-GD = Pre-grain-dissolution porosity (=Pre-PLC - PLC); Pre-QC = Pre-quartz-cement porosity (=Pre-GD + GD); Pre-LSC = Pre-late-stage-cements porosity (=Pre-QC - QC); Post-LSC = Post-late-stage-cements porosity (=Pre-LSC - LSC).

Diagenetic types	Wells	Depth/m	Detrital grains/%						Ma/%	Cements/%						TSP/%		DC/%	DP/%	GCC/%	Depositional facies	Diagenetic types
			Q	F	L		Mi	HM		CC		QC	PLC	PFC		Intra	Inter					
					RL	DL				Intra	Inter			Intra	Inter							
Type A	Y-6	2194.45	34.2	17.2	6.5	0.3	10.5	0.9	0.0	3.4	8.6	0.6	11.1	0.6	1.2	3.1	1.8	10.8	7.1	94.5	DCS	Type A
	H-2	2135.81	33.3	18.6	11.1	2.6	5.2	1.0	0.3	2.3	4.9	1.6	11.1	0.7	1.6	1.6	3.9	8.2	4.6	94.2	DCS	
	Y-6	2197.61	40.1	19.1	3.7	2.5	10.8	0.6	0.0	1.5	3.7	0.6	8.6	0.6	2.2	4.3	1.5	13.3	6.5	89.4	DCS	
	Y-6	2194.49	26.0	21.9	12.9	0.6	12.9	0.3	0.3	3.8	1.5	1.8	11.4	0.3	0.9	3.8	1.8	13.7	7.9	95.8	DCS	
	Average A	–	33.4	19.2	8.5	1.5	9.8	0.7	0.2	2.8	4.7	1.2	10.6	0.5	1.5	3.2	2.3	11.5	6.5	93.5	–	
Type B	NG-2	1651.6	42.6	8.2	14.1	0.7	15.4	1.6	0.0	5.2	4.9	2.6	0.0	0.0	1.0	3.0	0.7	16.1	8.2	58.0	SDF	Type B
	X-7	1927.3	47.3	10.4	9.1	6.4	6.4	0.0	0.9	3.4	2.1	9.5	0.3	0.0	0.9	2.4	0.9	13.7	5.8	24.9	DCS	
	X-7	1967.3	43.0	8.4	10.4	2.4	16.7	0.0	0.0	2.7	3.0	6.0	1.2	0.3	2.1	2.1	1.8	19.1	5.1	36.3	DCS	
	X-7	1927.2	30.1	8.8	28.0	4.0	8.3	0.0	1.6	3.1	0.5	6.2	1.6	0.0	1.0	4.1	1.6	13.8	7.3	34.9	DCS	
	B-4	1941.4	36.9	3.8	21.5	3.8	17.3	0.0	0.0	3.8	1.5	5.0	0.0	0.0	0.0	3.1	3.1	21.2	6.9	56.8	SDF	
	ZH-5	2003	50.2	8.0	9.6	1.3	15.3	0.0	0.0	3.5	0.7	8.0	1.0	0.0	0.0	1.6	1.0	16.6	5.1	42.7	SDF	
	X-7	1982.3	37.8	2.6	23.8	3.5	9.2	0.0	1.5	3.1	0.0	9.2	1.0	0.0	0.5	6.6	0.5	14.2	9.7	18.9	TC	
	L-8	2284.5	42.5	5.8	19.5	4.0	10.2	0.0	0.0	2.2	0.9	7.5	0.4	0.0	0.0	5.8	1.3	14.2	8.0	30.6	TC	
	NG-2	1633.4	44.5	13.0	11.6	5.5	10.5	0.5	2.0	0.0	1.5	6.0	1.5	0.0	0.5	3.0	0.0	18.0	3.0	41.4	SDF	
	Average B	–	41.6	7.7	16.4	3.5	12.1	0.2	0.7	3.0	1.7	6.7	0.8	0.0	0.7	3.5	1.2	16.3	6.6	38.3	–	
Type C	HG-4	2517.57	37.6	22.3	5.4	1.0	15.3	0.0	1.0	2.5	1.0	7.4	2.0	2.0	1.5	1.0	0.0	17.3	5.4	36.2	MB	Type C
	L-4	1913.36	30.8	10.4	26.9	8.0	15.4	0.0	0.5	0.5	4.0	3.0	0.5	0.0	0.0	0.0	0.0	23.9	0.5	58.5	SDF	
	NG-3	1674.6	31.0	3.3	36.1	2.4	14.3	0.0	1.0	2.4	1.0	5.2	0.5	0.0	2.4	1.0	0.0	17.6	3.3	44.2	SDF	
	CH-1	1928.25	34.0	3.9	34.3	9.8	10.7	0.0	1.0	0.0	1.0	4.4	1.0	0.0	0.0	0.0	0.5	21.5	0.0	38.5	IB	
	L-8	2262.5	34.7	4.0	29.7	6.9	11.9	0.0	0.0	4.5	1.5	5.4	1.0	0.0	0.0	0.5	0.0	18.8	5.0	57.0	TC	
	NG-3	1674.5	47.0	8.2	11.0	1.9	15.1	0.0	2.5	5.3	2.6	2.2	0.9	0.3	2.2	0.0	0.6	19.6	5.6	65.1	SDF	
	B-4	1949.61	27.2	13.3	28.9	6.0	10.8	0.0	3.6	1.0	1.0	4.6	1.0	0.0	0.5	1.0	0.0	20.3	2.1	45.4	TC	
	NG-3	1621.24	41.5	8.4	14.2	0.6	15.5	0.0	2.2	6.0	1.4	5.9	1.2	0.0	0.0	2.5	0.6	18.3	8.5	30.3	IB	
	NG-3	1621.6	32.4	4.3	32.4	7.7	11.1	0.5	0.5	2.4	1.4	6.8	0.0	0.0	0.0	0.5	0.0	19.3	2.9	26.4	IB	
	ZH-7	2000.1	24.5	10.3	37.3	4.4	13.7	0.0	0.0	4.4	1.5	2.9	0.5	0.0	0.0	0.0	0.5	18.1	4.4	63.9	IB	
	ZH-10	1744.65	19.1	30.7	20.5	1.4	12.1	0.0	1.0	1.0	4.0	3.0	3.0	0.0	1.0	1.5	0.5	14.5	2.5	67.4	SDF	
	ZH-1	1863.76	42.0	13.0	18.4	6.5	10.0	0.0	2.5	0.5	2.0	1.5	1.0	0.0	2.0	0.0	0.0	19.0	0.5	76.5	SDF	
	ZH-1	1853.57	43.0	7.5	13.0	3.3	18.6	0.0	0.7	0.0	7.2	4.9	0.7	0.0	0.0	0.7	0.7	22.5	0.7	56.1	TC	
	NG-3	1716.3	31.4	8.1	32.9	12.4	5.2	0.0	1.4	1.0	1.0	6.2	0.5	0.0	0.0	0.0	0.0	19.0	1.0	66.5	SDF	
	ZH-10	1741.85	37.0	23.5	5.5	1.0	21.0	0.0	0.0	1.0	2.0	3.0	3.0	0.0	3.0	0.0	0.0	22.0	1.0	78.0	SDF	
	T-1	1687.15	36.1	19.6	10.8	0.5	16.0	0.5	1.0	2.6	5.2	4.1	2.1	0.0	0.0	0.0	0.0	17.5	2.6	67.9	IB	
	Average C	–	34.3	11.9	22.3	4.6	13.5	0.1	1.2	2.2	2.3	4.4	1.2	0.1	0.8	0.5	0.2	19.3	2.9	54.9	–	

Diagenetic types	Wells	Depth/m	Mz/μm	So	Permeability/mD	Porosity/%	Porosity evolution/%							Diagenetic types
							OP	COPL	Pre-PLC	Pre-GD	Pre-QC	Pre-LSC	Post-LSC (=TSP)	
Type A	Y-6	2194.45	206.8	1.5	0.09	11.4	35.7	16.1	23.4	12.3	19.4	18.8	4.9	Type A
	H-2	2135.81	180.6	1.6	0.22	9.6	35.0	15.0	23.2	12.1	16.7	15.0	5.6	
	Y-6	2197.61	166.3	1.7	0.07	11.2	34.0	20.8	16.7	8.0	14.5	13.9	5.9	

(*continued on next page*)

Table 2 (*continued*)

Diagenetic types	Wells	Depth/m	Mz/μm	So	Permeability/mD	Porosity/%	Porosity evolution/%							Diagenetic types
							OP	COPL	Pre-PLC	Pre-GD	Pre-QC	Pre-LSC	Post-LSC (=TSP)	
	Y-6	2194.49	197.9	1.8	0.09	11.4	34.0	19.9	17.3	5.8	13.7	12.0	5.6	
	Average A	–	187.9	1.7	0.1	10.9	34.7	18.0	20.1	9.6	16.1	14.9	5.5	
Type B	NG-2	1651.6	124.1	1.4	0.66	8.1	36.8	30.4	9.2	9.2	17.4	14.8	3.6	Type B
	X-7	1927.3	161.7	1.5	0.45	10.6	36.5	25.7	13.7	13.4	19.2	9.8	3.4	
	X-7	1967.3	124.1	1.7	0.21	10.4	34.6	23.9	14.0	12.8	17.9	11.9	3.9	
	X-7	1927.2	125.4	1.5	0.59	10.5	36.3	27.3	10.9	9.3	16.6	10.4	5.7	
	B-4	1941.4	151.8	1.6	0.06	9.9	35.5	28.7	9.6	9.6	16.5	11.5	6.2	
	ZH-5	2003	111.5	1.7	0.37	11.4	34.4	26.7	10.6	9.6	14.7	6.7	2.6	
	X-7	1982.3	144.3	1.7	0.12	10.0	34.3	24.7	11.2	10.2	19.9	10.7	7.1	
	L-8	2284.5	132.7	1.8	0.11	9.9	33.9	26.4	10.2	9.7	17.7	10.2	7.1	
	NG-2	1633.4	152.3	1.8	0.25	9.5	33.9	25.3	9.5	8.0	11.0	5.0	3.0	
	Average B	–	136.4	1.6	0.3	10.0	35.1	26.5	11.0	10.2	16.8	10.1	4.7	
Type C	HG-4	2517.57	115.0	1.5	0.05	6.8	36.1	26.7	11.9	9.9	15.3	7.9	1.0	Type C
	L-4	1913.36	97.1	1.4	0.02	5.7	37.0	31.5	7.5	7.0	7.5	4.5	0.0	
	NG-3	1674.6	98.8	1.5	0.03	8.0	36.2	29.2	9.0	8.6	11.9	6.7	1.0	
	CH-1	1928.25	98.0	1.5	0.08	7.1	36.0	30.6	6.8	5.8	5.8	1.5	0.5	
	L-8	2262.5	118.5	1.5	0.04	6.2	36.1	30.6	7.9	6.9	11.9	6.4	0.5	
	NG-3	1674.5	99.4	1.5	0.03	8.2	36.0	28.1	8.5	7.6	13.2	11.0	0.6	
	B-4	1949.61	114.0	1.5	0.03	7.6	36.0	28.3	7.2	6.2	8.2	3.6	1.0	
	NG-3	1621.24	122.7	1.7	0.03	7.8	34.4	26.0	9.1	7.9	16.4	10.5	3.1	
	NG-3	1621.6	110.1	1.7	0.03	6.9	34.3	28.1	8.2	8.2	11.1	4.3	0.5	
	ZH-7	2000.1	116.5	1.7	0.03	7.8	34.2	30.4	5.4	4.9	9.3	6.4	0.5	
	ZH-10	1744.65	100.5	1.9	0.01	6.6	33.3	23.7	11.6	8.5	11.1	8.0	2.0	
	ZH-1	1863.76	108.1	2.0	0.01	4.0	32.6	26.0	6.5	5.5	6.0	4.5	0.0	
	ZH-1	1853.57	90.1	1.9	0.02	5.3	32.9	22.0	13.4	12.7	13.4	8.5	1.3	
	NG-3	1716.3	129.3	1.7	0.01	4.7	34.8	28.3	7.6	7.1	8.1	1.9	0.0	
	ZH-10	1741.85	97.5	1.7	0.01	5.3	34.5	26.4	11.0	8.0	9.0	6.0	0.0	
	T-1	1687.15	89.4	1.6	0.01	3.8	35.6	26.5	11.3	9.3	11.9	7.7	0.0	
	Average C	–	106.6	1.6	0.0	6.4	35.0	27.6	8.9	7.8	10.6	6.2	0.7	

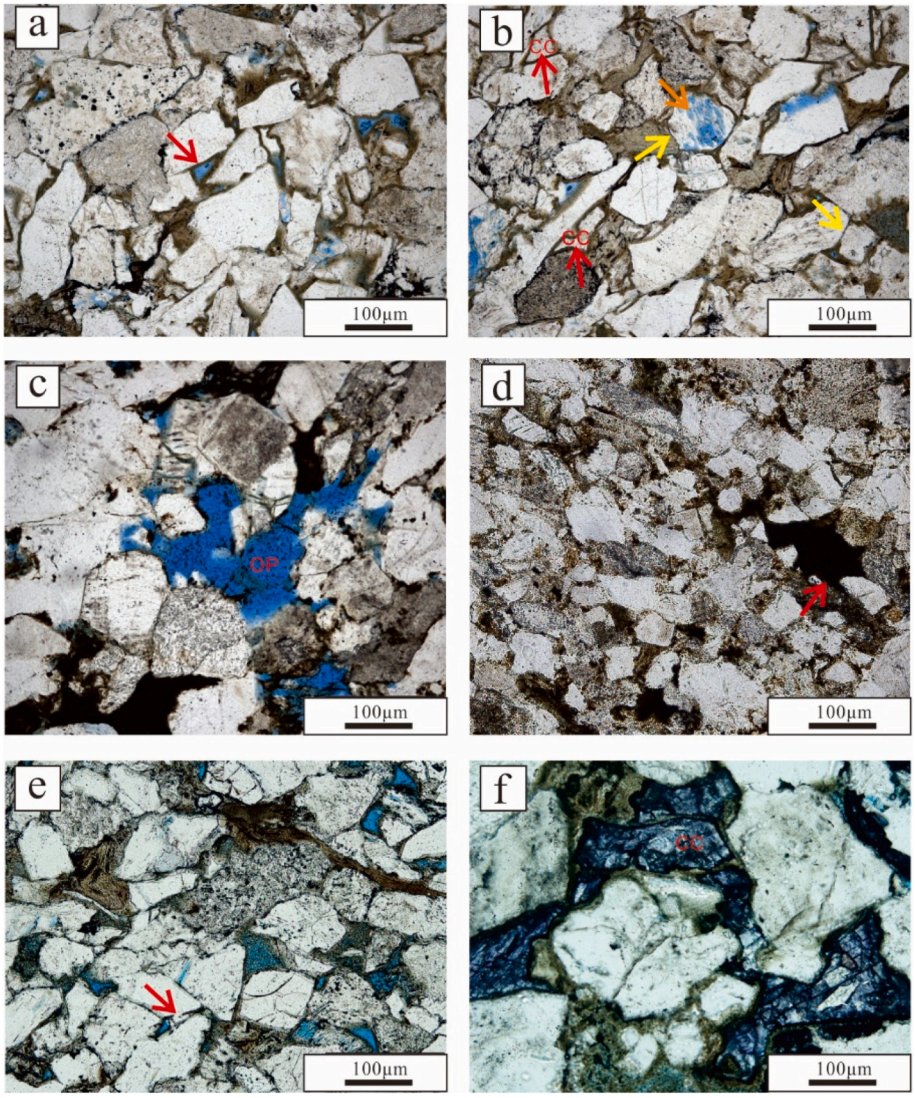

Fig. 7. Polarized light microphotographs of pore types and diagenetic features in the Chang 7 sandstones. a) Regularly triangular primary intergranular pores (red arrow). b) Clay coatings are present along the contact surfaces between grains (yellow arrow). Intragranular pores result from feldspars dissolution are observed (orange arrow). Some intergranular pores are filled with carbonate cements (red arrow). c) Oversized pores resulting from the intense dissolution of sedimentary material are observed. d) Ductile components undergo intense plastic deformation, they are squeezed and extruded between more rigid grains, reflecting low mechanical stability (red arrow). e) Quartz cement occurs preferentially where chlorite rims are discontinuous (red arrow). f) Dissolution pores are occupied by carbonate cements. CC = Carbonate cements; QC = Quartz cement; OP = Oversized pores.

pores and cements filling in intragranular pores (i.e., = Intra TSP + Intra CC + Intra PFC, see Table 2).

Intergranular and intragranular pores are main types of pores and usually with a range of 20–150 μm in size. Oversized pores are rare and normally 200–300 μm in size.

4.4. Diagenetic alterations

The Chang 7 sandstones showed advanced diagenetic alterations. Ductile components usually undergo intense plastic deformation, and are squeezed and extruded between more rigid grains during compaction (Fig. 7d).

In addition to compaction, cementation is another factor leading to porosity reduction. The prevalent cements include quartz, carbonate, and clay minerals. Quartz cement ranges from 0.6% to 9.5% with an average of 4.7%. It usually occurs as overgrowth around detrital quartz grains, and occurs preferentially where chlorite rims or coatings are discontinuous (Fig. 7e). In areas of completely grain coated quartz grains syntaxial overgrowth cements are absent. Carbonate cements (with an average content of 5.0%) in the study area are dominated by calcite, ferroan calcite, and ankerite according to the stained thin section observation and EDS analysis. For stained thin section, calcite appears red, ferroan calcite purple (Fig. 7f), and ankerite blue. Carbonate cements often occupy the intergranular pores and dissolution pores (Fig. 7f). Clay minerals mainly include chlorite, kaolinite, and illite. Pore-lining clay minerals (mainly chlorite rim, with an average content of 2.3%) are present on the outlines of detrital grains, they are also found along the contact surfaces between grains (Fig. 7b). Pore-filling clay minerals are present with an average content of 1%, often occupy intergranular pores and dissolution pores. Occasionally, pore-filling clay minerals replacing the entire detrital grains are also observed.

Secondary porosity (ranges from 0 to 6.6% with an average of 1.8%) due to grain dissolution is usually observed. It is mainly related to the dissolution of feldspar grains and volcanic rock fragments. Secondary pores are sometimes filled with pore-filling clays or carbonate cements.

4.5. Authigenic chlorite

4.5.1. Morphology of authigenic chlorite

The authigenic chlorites in the study area are primarily pore-lining chlorite and pore-filling chlorite. In addition, two main types of pore-lining chlorite have been observed: thin coatings made of poorly crystallized aggregates are directly in contact with quartz grains and overgrown by more euhedral, thicker rims (Fig. 8a and b). These coatings were preserved along the intergranular contact areas (Fig. 7b). Meanwhile, the outer chlorite rims are made of platelets arranged edge-to-face (Fig. 8a), covering the underlying coatings. In general, these rims have nearly equal thicknesses (approximately 3–10 μm; Fig. 8b). The grain coat coverage ranges from 18.9% to 95.8% with an average of 55% (Table 2).

Grain-replacing chlorite usually replaces detrital grains, such as feldspars or rock fragments (Fig. 8c). Occasionally, chlorite rosettes (Fig. 8d) and double chlorite rims covering both sides of the clay coatings were observed in some dissolved grains (Fig. 8c and d). Pore-filling chlorite also occur in intergranular pores as chlorite rosettes (Fig. 8b).

4.5.2. Mineralogy of authigenic chlorite

The mineralogy of the clay samples (<2 μm) reveals a well-crystallized 14 Å chlorite and a poorly crystallized 10 Å illite (Fig. 9). Chlorite was recognized by its characteristic (001) (14.18 Å), (002) (7.09 Å), (003) (4.72 Å), and (004) (3.54 Å) peaks (Fig. 9). As shown in the XRD patterns, chlorite exhibits relatively low intensities of the d (001) and d (003) peaks to the d (002) and d (004) reflections. The ethylene glycol saturated samples showed no obvious change compared to the air-dried samples. An increase in the intensity of the peak at approximately 14 Å relative to the other peaks was observed in the heat-treated sample (Fig. 9); this increase occurred because chlorites dehydroxylate after heating to 550 °C (Hillier, 2003).

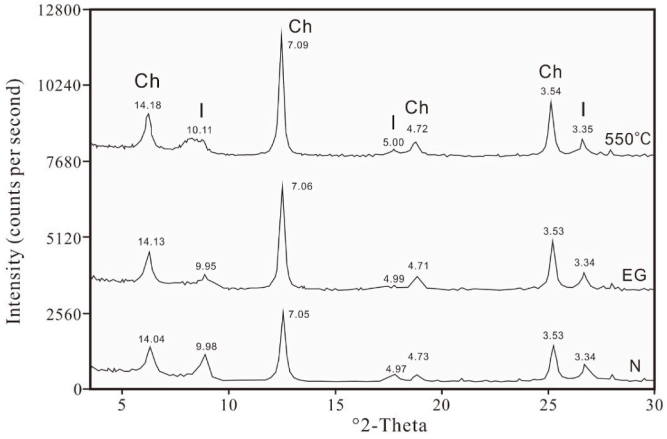

Fig. 9. X-ray diffraction patterns of clay fraction (<2 μm) of sample well HG1, 2524.53 m. A well-crystallized 14 Å chlorite and a poorly crystallized 10 Å illite were identified. Ch - Chlorite; I - Illite; N - air-dried sample; EG - ethylenglycol saturated sample; 550 °C - sample heated to 550 °C.

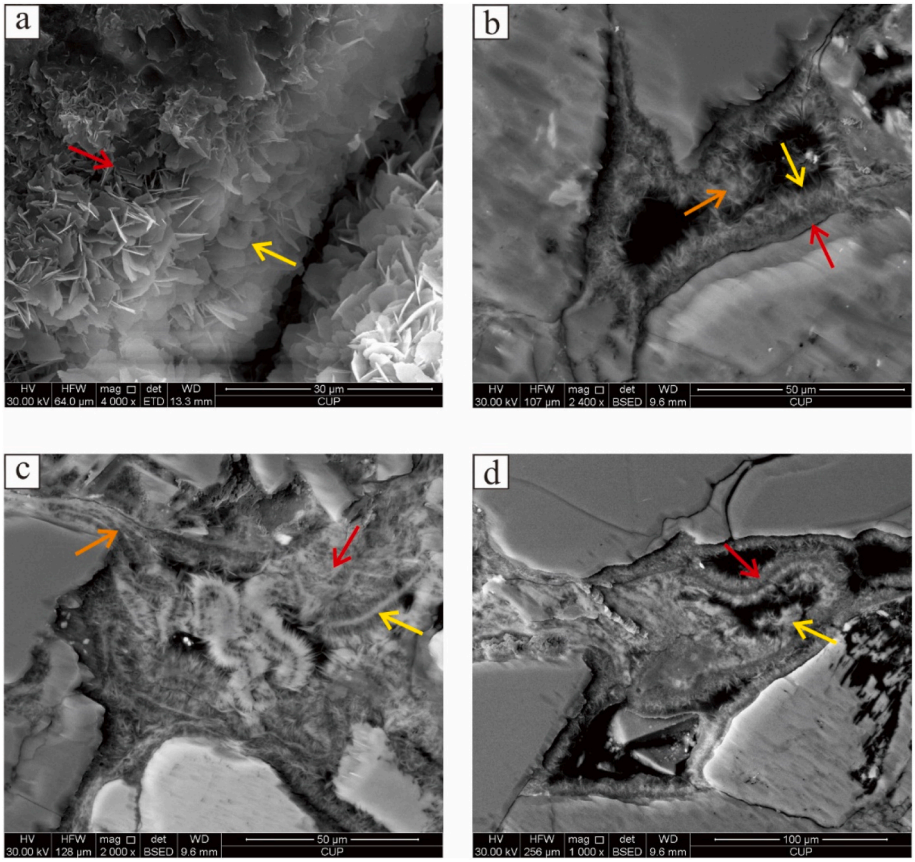

Fig. 8. BSE microphotographs of authigenic chlorite in the Chang 7 sandstones. a) thin coatings made of poorly crystallized aggregates (red arrow) are directly in contact with quartz grains and overgrown by more euhedral, thicker rims (yellow arrow). b) The thin coatings (red arrow) are covered by isopachous authigenic chlorite rims (yellow arrow). Chlorite rosettes (orange arrow) seem to occur in the growth of the outer part of the chlorite rims. c) Grain replacive chlorite replacing detrital grains (red arrow). Double chlorite rims cover both sides of the coating (yellow arrow). The chloritization of biotite appeared to occur along the trace of cleavage planes (orange arrow). d) Double chlorite rims (red arrow) cover both sides of the clay coating after grain dissolution. Chlorite rosettes partly occupy the intragranular dissolution pores (yellow arrow).

4.6. Diagenetic types

Three different diagenetic types could be identified according to the specific diagenetic features (Fig. 10). Type A sandstones were characterized by abundant authigenic chlorite rims, rare quartz cement, abundant carbonate cements, and relatively high porosity (generally >10%). Type B sandstones had a similar current porosity to Type A, but their diagenetic features were quite different. They generally have few chlorite rims, abundant quartz cement, and limited carbonate cements. Type C sandstones were characterized by abundant ductile components, intense compaction, and low porosity (generally 4%–8%).

4.7. Porosity and permeability

The core porosity of the sandstones ranges from 3.8% to 11.4%, with an average of 8.1%. The core air permeability ranges from 0.01 to 0.66 mD, with an average of 0.13 mD. A good correlation was observed between porosity and permeability (Fig. 11) ($R^2 = 0.61$). Type A and Type B sandstones are usually of good quality, with relatively high porosity and permeability. Type C sandstones are mainly characterized by poor petrophysical properties.

Correlation analysis showed that detrital components and cements had little correlation with porosity. This indicates that the porosity may be controlled by multiple factors, and that no single factor decisively influences the final porosity.

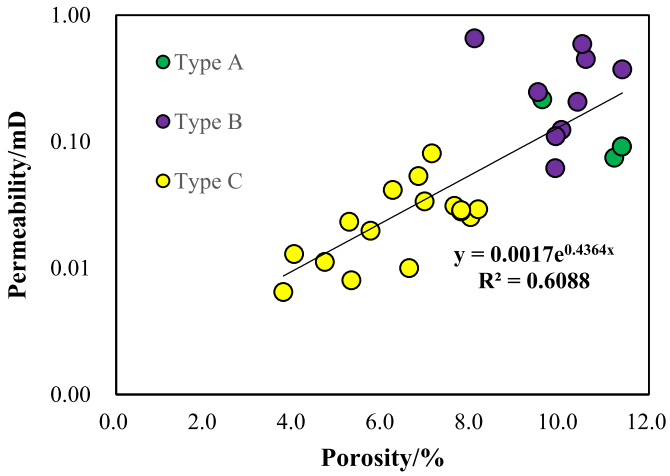

Fig. 11. Relationship between porosity and permeability of the Chang 7 sandstones.

5. Discussion

5.1. Interpretations of lithofacies

Lithofacies 1–3 reflect a delta front background. In this study, three main depositional microfacies could be distinguished in the delta front environment (Fig. 4): distributary channels (DC), inter-distributary bays (IB), and mouth bars (MB). Lithofacies 1 is interpreted as distributary channel (DC) deposits, whereas underlying mudstones is interpreted as interdistributary bay (IB) deposits. Lithofacies 3 is interpreted as Mouth bar (MB) deposits, they are rare in our observations.

Dark mudstones containing some fish fossils (Lithofacies 6) are extensively developed, indicating that they are deep-water deposits under quiet water conditions. On the other hand, thick sandstone bodies (Lithofacies 4–5) directly overlain and sealed by thick mudstones (Lithofacies 6) are interpreted as deep-water deposits. In addition, numerous deformation structures developed in Lithofacies 4–5 also indicate the presence of deep-water deposits in a gravity flow setting. Above all, Lithofacies 4–6 are interpreted as deep-water gravity flow deposits. Gravity flow deposits in the study area mainly include sandy debris flow (SDF) and turbidity current (TC) (Fig. 4). Lithofacies 4 is interpreted as sandy debris flow deposits in a deep-lacustrine setting, reflecting a plastic rheology and laminar flow state (Shanmugam, 1997; Talling, 2013). Similar observations and interpretations of these massive sandstones have been widely reported in previous studies on the Ordos Basin (Zou et al., 2012; Yang et al., 2014; Xu et al., 2016; Sun et al., 2020). Lithofacies 5 is interpreted as turbidity current deposits. Sandstones formed by turbidity currents usually display various bedding characteristics, and may show different vertical stacking patterns and display incomplete Bouma sequences, reflecting a turbulent flow with Newtonian rheology (Lowe, 1982; Shanmugam and Moiola, 1995; Haughton et al., 2009).

5.2. Paragenetic sequence of diagenesis

Compaction causes the rearrangement and deformation of detrital grains, which leads to the reduction of sandstone porosity. This process usually occurs in eogenetic stage. Thin section observations show that pore-lining clays were preserved along the intergranular contact areas (Fig. 7b), suggesting that they formed before a certain amount of compaction. Chlorite rims can inhibit the formation of quartz overgrowths, indicating that the quartz overgrowths form after chlorite rims. In our previous work (Dou et al., 2018a), we reported the homogenization temperature for aqueous inclusions in quartz overgrowths, which showed that the formation temperature of quartz overgrowths was about 85–130 °C. Grain dissolution is generally thought to be associated with the formation of organic acids and occurs mainly in the early stages of mesogenesis. In our observations, chlorite rims often outline the edges of the pre-dissolution grains, suggesting that dissolution occurs after the

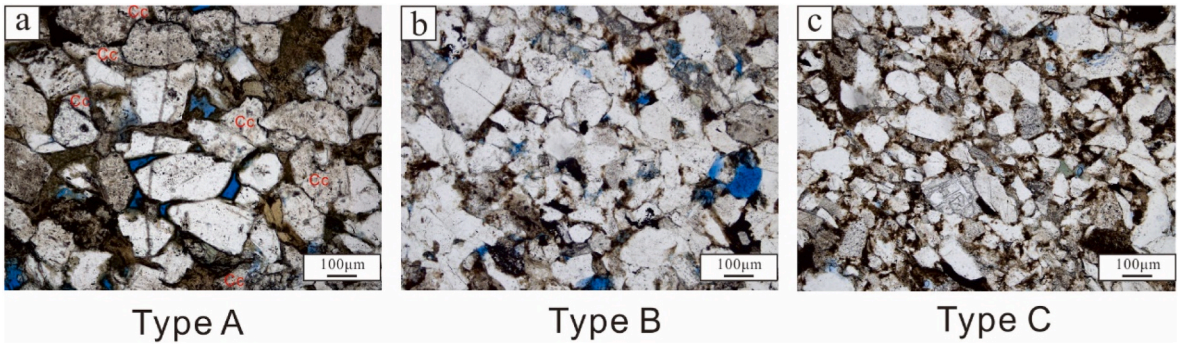

Fig. 10. Three different diagenetic types of the Chang 7 sandstones. Type A sandstones were characterized by abundant authigenic chlorite rims, rare quartz cement, abundant carbonate cements, and relatively high porosity. Type B sandstones had a similar current porosity to Type A, they generally have few chlorite rims, abundant quartz cement, and limited carbonate cements. Type C sandstones were characterized by abundant ductile components, intense compaction, and low porosity. Cc = Carbonate cements.

formation of chlorite rims. In addition, late-stage cements (pore-filling clays and carbonate cements) usually fill the dissolution pores, indicating that dissolution predates the formation of these cements. According to our previous study (Dou et al., 2018a), combined with the homogenization temperature for aqueous inclusions and isotope data, the formation temperature of carbonate cements is about 100–140 °C. We do not have additional data on the specific formation temperature of late-stage clays, but based on diagenetic sequences, the formation of late-stage clays postdates the grain dissolution. In this study, we speculate that late-stage clays and late-stage carbonate cements may form at the same time. The diagenetic sequences of the sandstones studied are summarized in Fig. 12.

5.3. Origin of authigenic chlorite

Thin coatings preserved along intergranular contact areas were commonly observed, suggesting that they formed before a certain amount of compaction. These pre-compactional coatings may be related to riverine water influx (Zhang et al., 2011; Chen et al., 2014) or the alteration of volcanic materials (De Ros et al., 1997; Humphreys et al., 1994). However, there was no significant difference in the ferromagnesian mineral (including biotite and volcanic materials) contents between the chlorite-rich and chlorite-free samples, indicating that the development of chlorite coatings may not be related to the hydrolysis of ferromagnesian minerals. Furthermore, sandstones rich in chlorite rims usually occur in distributary channels (Table 2) and are relatively coarse-grained, reflecting a high-energy hydrodynamic environment during the depositional period. This result indicates that the formation of chlorite rims is likely controlled by the sedimentary environment. Therefore, it is more likely that these coatings are related to riverine water influx. Where the river enters the lake, hydrolysis and dissolution of the flocculated iron-rich colloforms that formed during the sedimentary period can provide abundant iron and magnesium to form chlorite (Chen et al., 2014; Zhu et al., 2017).

The chlorite rims covering the coatings were mostly isopachous, suggesting that they were of diagenetic origin. The relatively low intensities of the d (001) and d (003) peaks to the d (002) and d (004) reflections as shown in XRD, indicating that chlorite is Fe enriched (Moore and Reynolds, 1997). Chlorite coatings can provide a substrate for the growth of chlorite rims under conditions of Fe- and Mg-rich pore waters, which could be derived from the hydrolysis of ferromagnesian minerals such as biotite and volcanic materials (Zhang et al., 2011; Chen et al., 2014). The chloritization of biotite is observed in this study (Fig. 8c). Diagenetic features from thin-sections reveal that pore-filling chlorite generally postdated the growth of chlorite rims and grain dissolution (Fig. 8c and d). Thus, the materials needed for their formation must be derived from grain dissolution and compactional fluids from adjacent shales (Zhang et al., 2011; Chen et al., 2014).

5.4. Factors influencing porosity alteration

All sandstones in this study area underwent similar diagenetic processes shown as Fig. 12, but the degree varied widely among different types of sandstones. Three different diagenetic types were identified, showing very different diagenetic evolution pathways (Fig. 13). Compaction and cementation can result in porosity reduction and dissolution can result in porosity enhancement. The amount of porosity variation due to specific diagenetic event are calculated based on thin section analysis and details can refer to Table 2.

5.4.1. Compaction

To account for bulk volume changes, compactional porosity loss (COPL) was used to evaluate the porosity loss due to compaction (Ehrenberg, 1989). Ductile components usually play an important role in reducing porosity during compaction, as they can be largely deformed and squeezed between more rigid grains during compaction. As shown in Fig. 14a, the ductile component content had a positive correlation with the level of porosity lost due to compaction. This finding indicates that sandstones with larger quantities of ductile components usually lose more primary porosity than those with smaller quantities because of the increased compaction effects (Paxton et al., 2002).

Another important factor that affects compaction is grain size. As shown in Fig. 14b, the grain size had a negative correlation with the COPL, indicating that coarser-grained sandstones lose porosity to a lesser extent during compaction than fine-grained sandstones. This may explain why grain size correlates positively with porosity ($R2 = 0.51$, Fig. 14c).

Grain size and the ductile component content influence porosity alteration. To a certain extent, both of these factors are related to depositional environment. As shown in Fig. 14d, for sandstones deposited in a delta front setting, the grain size and ductile component content are largely controlled by the depositional environment. Sandstone deposits in distributary channels (DC) are relatively coarse-grained and contain less ductile components, reflecting a high-energy hydrodynamic environment. Conversely, sandstone deposits in interdistributary bays (IB) are relatively fine-grained and contain more ductile component content, reflecting a low-energy hydrodynamic environment. Sandstone deposits in mouth bars (MB) are of the transitional type, between

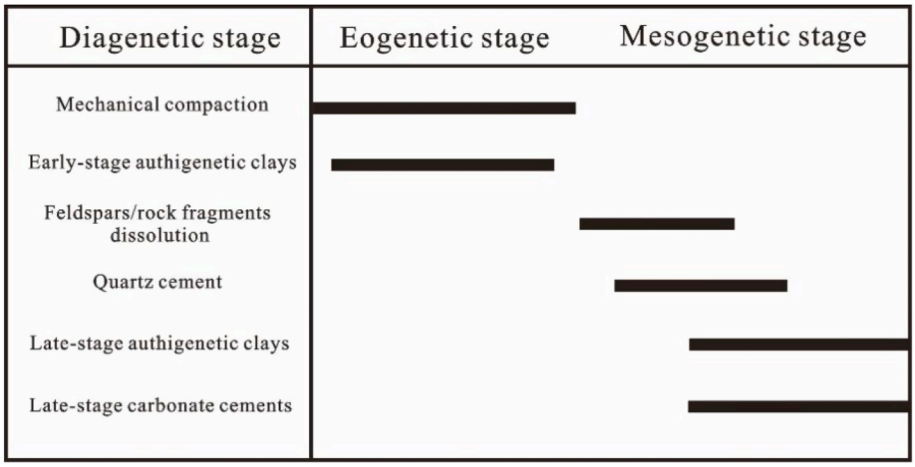

Fig. 12. Paragenetic sequence of the Chang 7 sandstones. Only the most significant diagenetic alterations affecting the sandstones are included. Early-stage authigenic clays mainly include pore-lining clays. Late-stage authigenic clays mainly include pore-filling clays. Late-stage carbonate cements mainly include ferrocalcite, ankerite, and calcite.

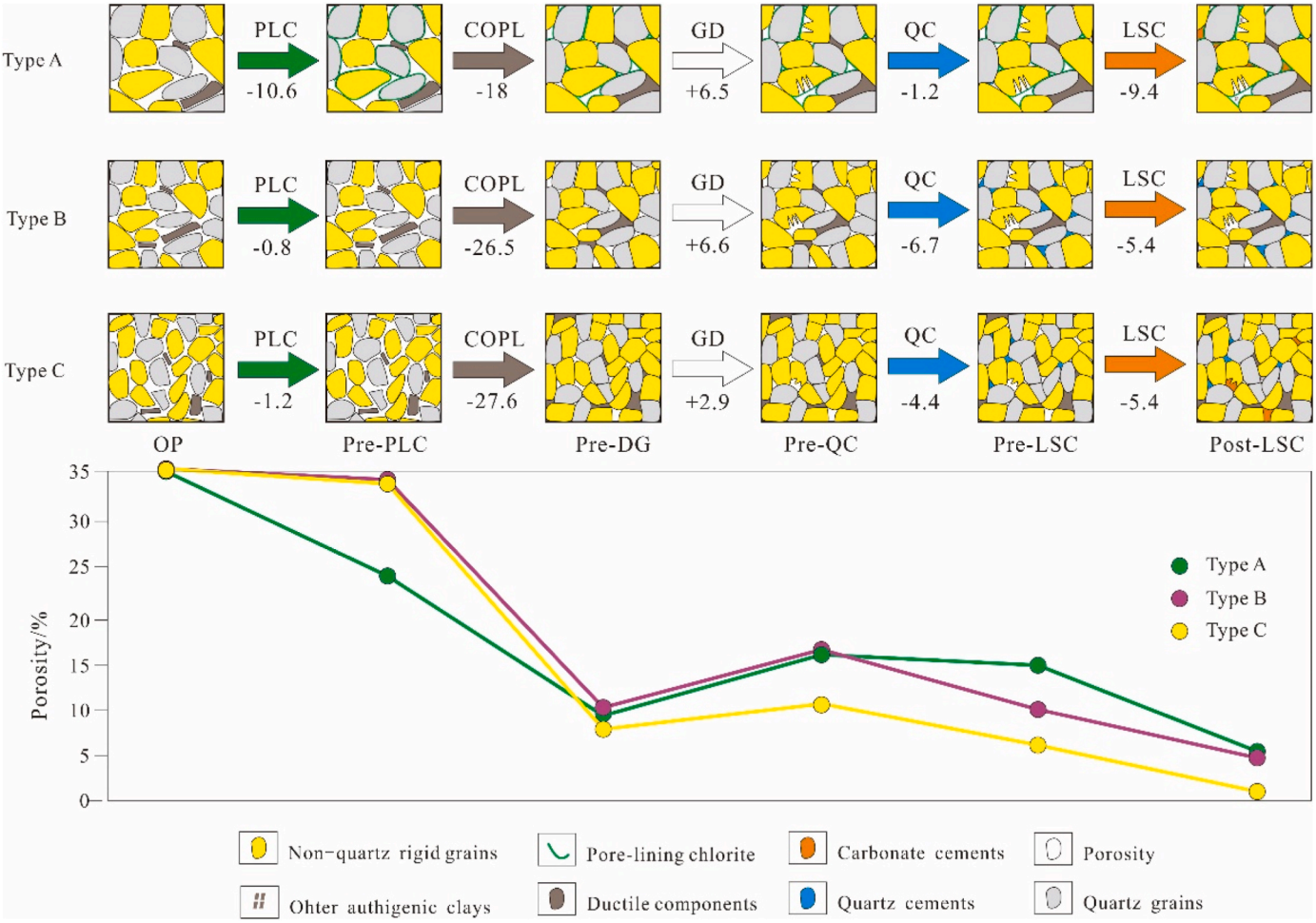

Fig. 13. A summary model of the diagenetic evolution pathways and corresponding porosity evolution of the Chang 7 sandstones. Type A sandstones were characterized by abundant authigenic chlorite rims, rare quartz cement, abundant carbonate cements and relatively high porosity. Type B sandstones generally have minimal chlorite rims, abundant quartz cement and limited carbonate cements. Type C sandstones were characterized by abundant ductile components, intense compaction and low porosity. Abbreviation and data sources refer to Table 2.

distributary channels (DC) and interdistributary bays (IB). However, for sandstones deposited in a gravity flow setting, the grain size and ductile components show no obvious differences between sandstones deposited in sandy debris flow (SDF) and turbidity current (TC). In general, sandstones of gravity flow origin reflect a relatively lower energy in hydrodynamic environment than those deposited in distributary channels (DC).

5.4.2. *Chlorite rims and its impact on porosity preservation*

To date, the mechanisms by which chlorite rims effectively inhibit quartz overgrowth are unclear. It is possible that chlorite rims inhibit quartz cement by isolating quartz grains from silica-saturated formation water (Barclay and Worden, 2000; Worden and Morad, 2000) or by inhibiting the epitaxial growth of quartz grains (Billault et al., 2003; Ajdukiewicz and Larese, 2012; Worden et al., 2020). However, it has been widely reported that chlorite rims can contribute to preserving porosity by inhibiting quartz cementation (Ehrenberg, 1993; Hillier, 1994; Pittman and Lumsden, 1968). Indeed, the development of chlorite rims can inhibit the formation of quartz overgrowths, which is well illustrated by the negative correlation between quartz cement content and grain coat coverage (Fig. 15).

5.4.3. *Late-stage cements*

Late-stage cementation is an important factor leading to porosity reduction and mainly includes late-stage authigenic clay minerals and late-stage carbonate cements. Herein, pore-filling kaolinite, illite, and chlorite rosettes were the main late-stage authigenic clay minerals, and the materials needed for their formation may have been derived from grain dissolution or compactional fluids from adjacent shales (Chen et al., 2014; Zhang et al., 2011).

Late-stage carbonate cements mainly include ferroan calcite, ankerite, and calcite, each of which could be related to the decarboxylation of organic matter or the dissolution of marine carbonate rock fragments (Wang et al., 2007; Sun et al., 2010; Dou et al., 2018a). The content of carbonate cements revealed a very good positive correlation with the available porosity at the time of their precipitation, suggesting that the diagenetic fluids preferentially passed through the more porous and permeable pathways within the sandstones, precipitating more carbonate cements (Dou et al., 2018a, 2018b).

5.4.4. *Porosity evolution*

For Type C sandstones, the porosity reduction was mostly controlled by intense compaction, cementation and dissolution had little impact on the porosity evolution. Before dissolution, the Type A and B sandstones had similar porosity, and during dissolution, they underwent similar porosity enhancements. After dissolution, the quartz cementation was inhibited by chlorite rims in the Type A sandstones, with an additional porosity of approximately 5.5% preserved for the chlorite-rich sandstones, as compared with the Type B sandstones, which lack chlorite (Fig. 13). However, sandstones with high porosity and permeability are

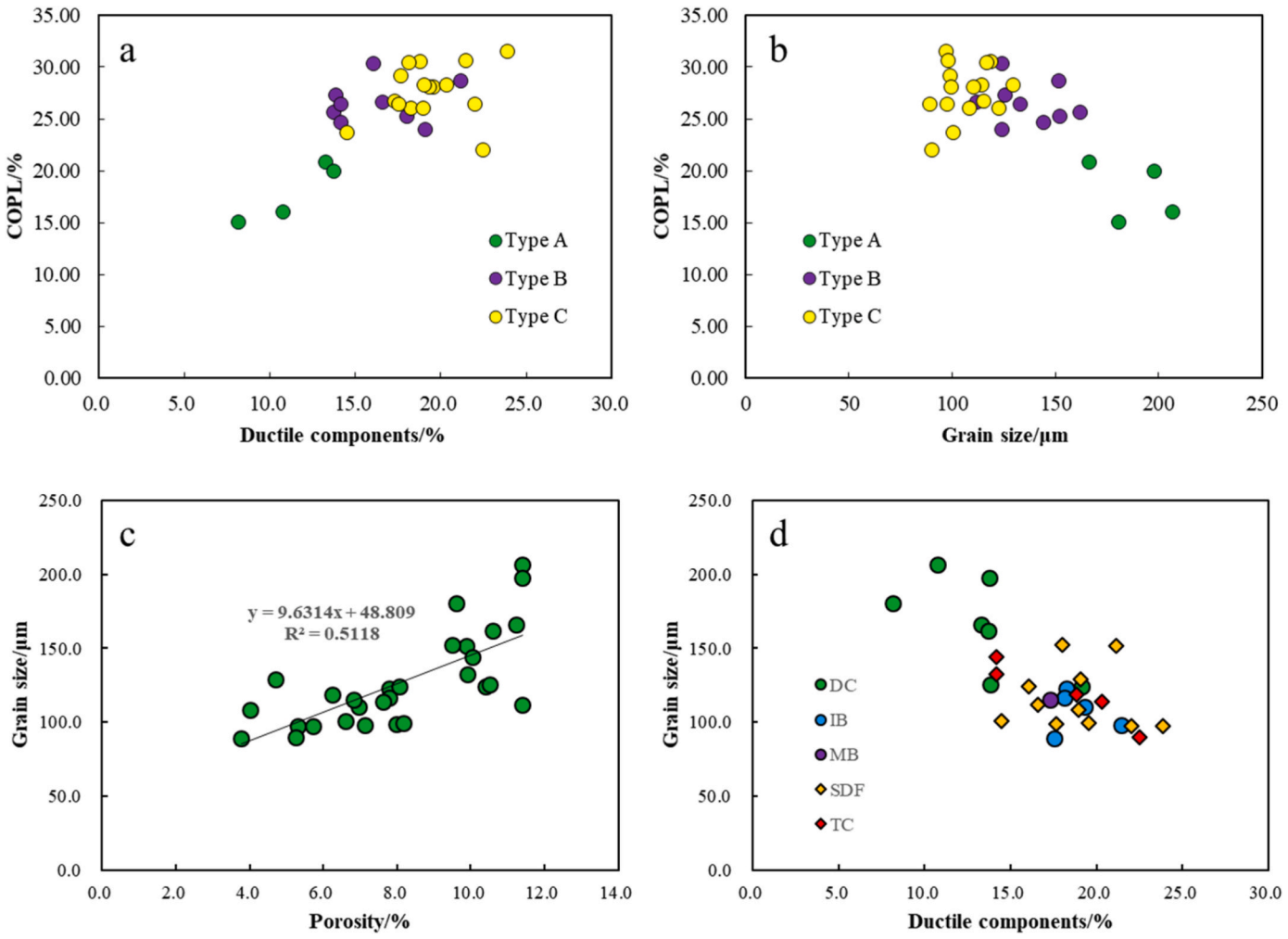

Fig. 14. a) Compactional porosity loss (COPL) versus ductile components. It indicates that compaction is largely controlled by the content of ductile components; b) COPL versus grain size. It indicates that compaction is controlled by the content of ductile components. Type A sandstones generally had the largest grain size, followed by Type B and Type C; c) The relationship between grain size and porosity; d) The relationship between grain size, ductile components and depositional environment.

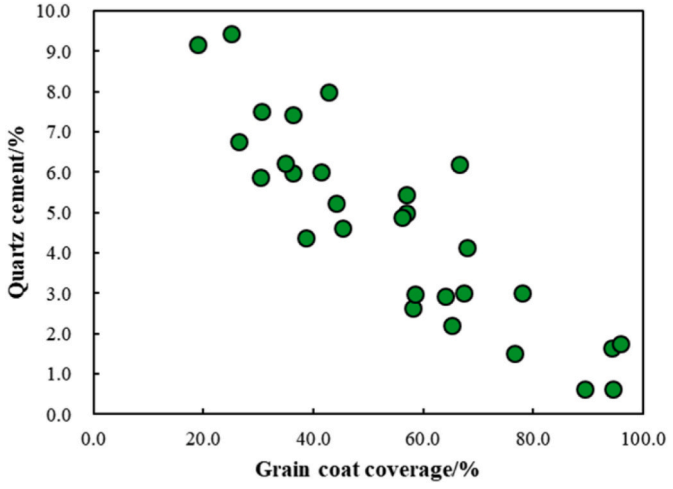

Fig. 15. Grain coat coverage versus quartz cement.

the preferential fluid flow pathways and preferred sites for mineral precipitation (Sullivan and McBride, 1991; Lynch, 1996; Dou et al., 2018b). At the time of late-stage cementation, Type A sandstones provided more available porosity for mineral precipitation and developed more cements than Type B sandstones. Consequently, the porosity preserved by chlorite rims in the Type A sandstones was almost completely destroyed by late-stage cementation, and a similar current porosity was observed between the Type A and B sandstones (Fig. 13).

5.5. *Efficacy of chlorite rims in preserving porosity: how important are chlorite rims for porosity preservation?*

Sandstone porosity generally decreases with increasing burial depth and gradual compaction and cementation processes. These diagenetic processes of porosity reduction can be disassembled chronologically into processes such as compaction, quartz cementation and other late-stage cementation (e.g., carbonates and clays). However, compaction and cementation can be retarded, thereby preserving the porosity, as summarized in Table 3. Overall, quartz cementation is one of the many mechanisms that causes porosity reduction; by inhibiting quartz cementation, chlorite rims are able to preserve porosity. However, other factors, such as compaction and other cements, may not be retarded by chlorite rims. Therefore, these factors that may cause porosity reduction should also be considered when evaluating the degree of contribution of chlorite rims to porosity preservation.

Compaction generally occurs at an early stage and at shallow depths (generally <1500 m, Paxton et al., 2002). In sandstones in which

Table 3
Summary of mechanisms of porosity preservation.

Mechanisms of porosity preservation	Description	Example
Fluid overpressure at shallow depth	Retards compaction but has little effects on cementation	Scherer (1987); Ramm and Bjørlykke (1994)
Anomalously low temperature	Retards quartz cementation, which is largely controlled by temperature	Taylor et al. (2010)
Early emplacement of hydrocarbons	Retards cementation by isolating pore water from the rocks	Marchand et al. (2000), 2001, 2002; Worden et al., 1998; 2018
Grain coats and rims	Retards quartz cementation but cannot retard carbonate or clay cementation	Ehrenberg (1993); Hillier S, 1994; Bloch et al. (2002); Ajdukiewicz et al. (2010)

porosity reduction is largely controlled by compaction, mechanisms that inhibit cementation may have a smaller effect on porosity preservation because rare porosity remains after compaction. This is the case for Type C sandstones in this study in which limited cementation occurred because slight porosity remained after intense compaction. This is also supported by previous studies that indicate a reduced impact of chlorite rims on the porosity preservation of compositionally immature sandstones than mature ones (Pittman et al., 1992; Bloch et al., 2002; Bahlis and De Ros, 2013).

For sandstones with limited early compaction, porosity preservation would still depend on the degree of subsequent cementation. Chlorite rims are one of the important mechanisms inhibiting quartz cementation. Furthermore, chlorite rims usually develop in high-energy sandstones, which often have greater resistance to compaction than compositionally immature sandstones. This may explain why chlorite rims usually aid in porosity preservation. If there are no other late-stage cements, sandstones would preserve abnormally high porosity, even if they are deeply buried. For example, in the Garn Formation sandstones in the Norwegian continental shelf, as documented by Ehrenberg (1990, 1993), quartz cementation is the main factor resulting in porosity reduction. As expected, the cores in well 6406/3–1, which are rich in chlorite rims, had lower quartz cement abundance and higher porosity than the cores without chlorite rims.

Nevertheless, even if compaction and quartz cementation are both inhibited, other late-stage cementation processes (e.g., carbonates and clays) may play a role in porosity destruction. Our observations in this study show that chlorite rims do not prevent late-stage cements (LSC), such as carbonates and clays (Fig. 7f and 8b). Several previous studies have also indicated that these late-stage cements could not be inhibited by chlorite rims (Berger et al., 2009; Dutton et al., 2012; Zhang et al., 2012; Li et al., 2021). For Type A sandstones observed in this study, although quartz cementation was inhibited by chlorite rims, abundant porosity was subsequently destroyed by late-stage cements (avg. = 9.4%). In contrast, although Type B sandstones have few chlorite rims and thus underwent abundant quartz cementation, their late-stage cements were limited. Consequently, a similar current porosity was observed between the Type A and B sandstones. This means that the porosity preserved by chlorite rims in the Type A sandstones was almost completely destroyed by late-stage cementation, and chlorite rims have limited contribution to porosity preservation.

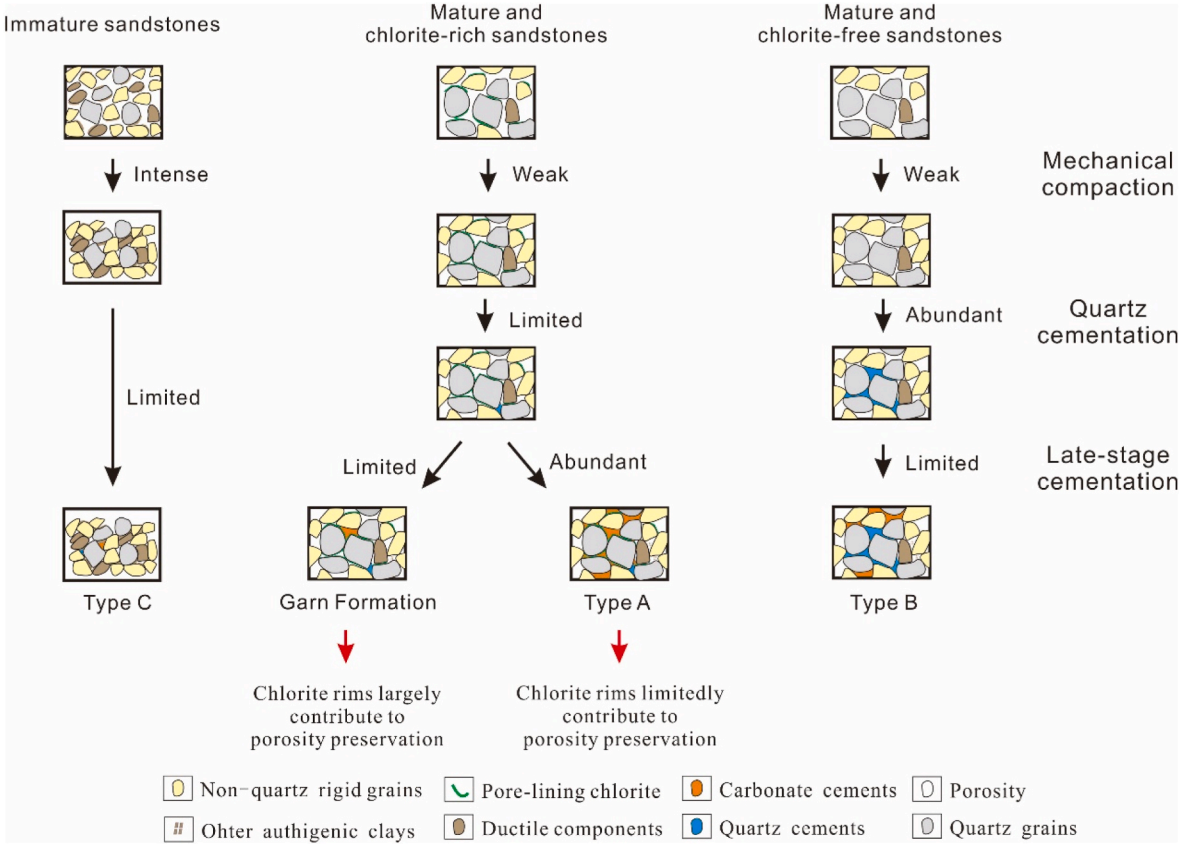

Fig. 16. Contribution degree of chlorite rims on porosity preservation under different scenarios. Limited cementation occurs in Type C sandstones because rare porosity remains after an intense compaction. As for Garn Formation sandstones in well 6406/3–1, as documented by Ehrenberg (1990, 1993), quartz cementation is the main factor resulting in porosity reduction. As expected, chlorite rims largely contribute to porosity preservation. Similar to Garn Formation sandstones, primary porosity in Type A sandstones preserves due to chlorite rims by inhibiting quartz cementation. However, most porosity loses by intense late-stage cementation, resulting in limited contribution of chlorite rims to porosity preservation. Compared with Type A, Type B sandstones have few chlorite rims and thus underwent abundant quartz cementation, but their late-stage cements were limited. Consequently, a similar current porosity was observed between the Type A and B sandstones.

The contribution of chlorite rims to porosity preservation under different scenarios is shown in Fig. 16.

6. Conclusions

The authigenic chlorite in the studied sandstones mainly includes pore-lining chlorite and pore-filling chlorite. In general, chlorite rims had nearly equal thicknesses (approximately 3–10 μm) and covered the underlying coatings. Furthermore, the sandstones rich in chlorite rims were mostly relatively coarse-grained, reflecting a high-energy hydrodynamic environment.

The diagenetic processes of porosity reduction can be disassembled chronologically into different processes, such as compaction, quartz cementation, and other late-stage cementation (e.g., carbonates and clays). Three different diagenetic types were identified according to specific diagenetic evolution pathways.

For Type C sandstones, the porosity reduction was mostly controlled by intense compaction, and the chlorite rims had little impact on porosity preservation. Type A and B sandstones had similar porosity before dissolution, and underwent similar porosity enhancements during dissolution. After dissolution, compared with Type B sandstones, Type A sandstones have limited quartz cements due to chlorite rims, but underwent more late-stage cementation. Consequently, a similar current porosity was observed between the Type A and B sandstones. This means that the porosity preserved by chlorite rims in the Type A sandstones was almost completely destroyed by late-stage cementation, and chlorite rims have limited contribution to porosity preservation.

The porosity preservation of sandstones is often controlled by many factors, and the effects of chlorite rims on porosity preservation are not always significant. Overall, chlorite rims play an important role in porosity preservation only in sandstones in which quartz cementation is the main process of porosity reduction.

Declaration of competing interest

The authors declare the following financial interests/personal relationships which may be considered as potential competing interests.

Data availability

Data will be made available on request.

Acknowledgements

This work was funded by the National Natural Science Foundation of China (Grant No. 42030808 and 41372143) and the Research Fund for the Doctoral Program of Higher Education (Grant no. 20130007110002). The authors are grateful to Luca Colombera for his careful editorial work. We are also grateful to Mark Wilkinson and several anonymous reviewers for the constructive comments.

References

Ajdukiewicz, J.M., Nicholson, P.H., Esch, W.L., 2010. Prediction of deep reservoir quality using early diagenetic process models in the Jurassic Norphlet Formation, Gulf of Mexico. AAPG (Am. Assoc. Pet. Geol.) Bull. 94 (8), 1189–1227.

Ajdukiewicz, J.M., Larese, R.E., 2012. How clay grain coats inhibit quartz cement and preserve porosity in deeply buried sandstones: observations and experiments. AAPG (Am. Assoc. Pet. Geol.) Bull. 96 (11), 2091–2119.

Bahlis, A.B., De Ros, L.F., 2013. Origin and impact of authigenic chlorite in the Upper Cretaceous sandstone reservoirs of the Santos Basin, eastern Brazil. Petrol. Geosci. 19 (2), 185–199.

Barclay, S.A., Worden, R.H., 2000. Geochemical modelling of diagenetic reactions in a subarkosic sandstone. Clay Miner. 35 (1), 57–67.

Beard, D.C., Weyl, P.K., 1973. Influence of texture on porosity and permeability of unconsolidated sand. AAPG (Am. Assoc. Pet. Geol.) Bull. 57, 349–369.

Berger, A., Gier, S., Krois, P., 2009. Porosity-preserving chlorite cements in shallow marine volcaniclastic sandstones: evidence from Cretaceous sandstones of the Sawan gas field, Pakistan. AAPG (Am. Assoc. Pet. Geol.) Bull. 93, 595–615.

Billault, V., Beaufort, D., Baronnet, A., Lacharpagne, J.C., 2003. A nanopetrographic and textural study of grain-coating chlorites in sandstone reservoirs. Clay Miner. 38 (3), 315–328.

Bloch, S., Lander, R.H., Bonnell, L., 2002. Anomalously high porosity and permeability in deeply buried sandstone reservoirs: origin and predictability. AAPG (Am. Assoc. Pet. Geol.) Bull. 86, 301–328.

Cai, P.T., 2019. The Research of Sandstone Diagenesis and Diagenetic Fluid of the Xujiahe Formation in the Central of Sichuan Basin. A Dissertation submitted to East China University on Technology for Master' Degree.

Chen, B.Y., Li, R.X., Liang, J.W., Huang, K.Z., 2014. Authigenic chlorite and its impaction on reservoir physical properties: an example from the Yanchang formation of the southwest Ordos Basin. Bull. China Soc. Mineral Petrol. Geochem. 33, 389–394 (in Chinese with English abstract).

De Ros, L.F., Morad, S., Al-Aasm, I.S., 1997. Diagenesis of siliciclastic and volcaniclastic sediments in the cretaceous and miocene sequences of NW african margin (DSDP leg 47A, site 397). Sediment. Geol. 112, 137–156.

Dou, W., Liu, L., Wu, K., Xu, Z., Feng, X., 2018a. Diagenesis of tight oil sand reservoirs: upper triassic tight sandstones of Yanchang Formation in Ordos Basin, China. Geol. J. 53, 707–724.

Dou, W., Liu, L., Wu, K., Xu, Z., Liu, X., Feng, X., 2018b. Diagenetic heterogeneity, pore throats characteristic and their effects on reservoir quality of the Upper Triassic tight sandstones of Yanchang Formation in Ordos Basin, China. Mar. Petrol. Geol. 98, 243–257.

Dowey, P.J., Hodgson, D.M., Worden, R.H., 2012. Pre-requisites, processes, and prediction of chlorite grain coatings in petroleum reservoirs: a review of subsurface examples. Mar. Petrol. Geol. 32 (1), 63–75.

Dutton, S.P., Loucks, R.G., Day-Stirrat, R.J., 2012. Impact of regional variation in detrital mineral composition on reservoir quality in deep to ultradeep lower Miocene sandstones, western Gulf of Mexico. Mar. Petrol. Geol. 35 (1), 139–153.

Editorial Committee of Petroleum Geology of Changqing Oilfield, 1992. Chinese Petroleum Geological Records. Petroleum Industry Press, Beijing, pp. 8–145 in Chinese.

Ehrenberg, S.N., 1989. Assessing the relative importance of compaction processes and cementation to reduction of porosity in sandstones: discussion; compaction and porosity evolution of Pliocene sandstones, Ventura Basin, California: discussion. AAPG (Am. Assoc. Pet. Geol.) Bull. 73, 1274–1276.

Ehrenberg, S.N., 1990. Relationship between diagenesis and reservoir quality in sandstones of the Garn Formation, haltenbanken, mid-Norwegian continental shelf. AAPG (Am. Assoc. Pet. Geol.) Bull. 74 (10), 1538–1558.

Ehrenberg, S.N., 1993. Preservation of anomalously high porosity in deeply buried sandstones by grain-coating chlorite; examples from the Norwegian continental shelf. AAPG (Am. Assoc. Pet. Geol.) Bull. 77 (7), 1260–1286.

Folk, R.L., 1968. Petrology of Sedimentary Rocks. Hemphill, Austin, TX, p. 107.

Guo, H.J., Jia, W.L., Peng, P.A., Lei, Y.H., Luo, X.R., Cheng, M., Wang, X.Z., Zhang, L.X., Jiang, C.F., 2014. The composition and its impact on the methane sorption of lacustrine shales from the Upper Triassic Yanchang Formation, Ordos Basin, China. Mar. Petrol. Geol. 57, 509–520.

Guo, K., Zeng, J.H., Liu, T.T., Lei, X., 2013. Hydrocarbon fluid flow stages and oil migration history in Yangchang Formation of Longdong area, Ordos Basin. Geoscience 27, 382–388 (in Chinese with English abstract).

Guo, X.W., Liu, K.Y., Jia, C.Z., et al., 2016. Effects of early petroleum charge and overpressure on reservoir porosity preservation in the giant Kela-2 gas field, Kuqa depression, Tarim Basin, northwest China. AAPG (Am. Assoc. Pet. Geol.) Bull. 100 (2), 191–212.

Haughton, P., Davis, C., McCaffrey, W., Barker, S., 2009. Hybrid sediment gravity flow deposits-Classification, origin and significance. Mar. Petrol. Geol. 26, 1900–1918.

Hillier, S., 1994. Pore-lining chlorites in siliciclastic reservoir sandstones: electron microprobe, SEM and XRD data, and implications for their origin. Clay Miner. 29 (4), 665–679.

Hillier, S., 2003. Quantitative analysis of clay and other minerals in sandstones by X-ray powder diffraction (XRPD). In: Worden, R.H., Morad, S. (Eds.), Clay Mineral Cements in Sandstones, Special Publication of the International Association of Sedimentologists. Blackwells, Oxford, pp. 213–252.

Humphreys, B., Kemp, S.J., Lott, G.K., Dharmayanti, D.A., Samsori, I., 1994. Origin of grain-coating chlorite by smectite transformation; an example from Miocene sandstones, North Sumatra back-arc basin, Indonesia. Clay Miner. 29, 681–692.

Lander, R.H., Walderhaug, O., 1999. Predicting porosity through simulating sandstone compaction and quartz cementation. AAPG (Am. Assoc. Pet. Geol.) Bull. 83, 433–449.

Lai, J., Wang, G., Chai, Y., et al., 2017. Deep burial diagenesis and reservoir quality evolution of high-temperature, high-pressure sandstones: examples from Lower Cretaceous Bashijiqike Formation in Keshen area, Kuqa depression, Tarim basin of China. AAPG (Am. Assoc. Pet. Geol.) Bull. 101 (6), 829–862.

Li, W.H., Pang, J.G., Cao, H.X., Wang, R.G., 2009. Depositional system and paleogeographic evolution of the late triassic Yanchang stage in Ordos Basin. J. NW Univ. 39, 501–506 (in Chinese with English abstract).

Li, X.B., Liu, H.Q., Pan, S.X., et al., 2018. Subaqueous sandy mass-transport deposits in lacustrine facies of the upper triassic Yanchang Formation, Ordos Basin, Central China. Mar. Petrol. Geol. 97, 66–77, 2018.

Li, K., Xi, K., Cao, Y., et al., 2021. Chlorite authigenesis and its impact on reservoir quality in tight sandstone reservoirs of the Triassic Yanchang Formation, southwestern Ordos Basin, China. J. Petrol. Sci. Eng. 205 (1), 108843.

Liu, Y., Qiu, N., Yao, Q., et al., 2016. Distribution, origin and evolution of the Upper Triassic overpressures in the central portion of the Sichuan Basin, SW China. J. Petrol. Sci. Eng. 146, 1116–1129, 2016.

Lowe, D.R., 1982. Sediment gravity flows: II. Depositional models with special reference to the deposits of high-density turbidity currents. J. Sediment. Res. 52, 279–297.
Lynch, F.L., 1996. Mineral/water interaction, fluid flow, and Frio sandstone diagenesis: evidence from the rocks. AAPG (Am. Assoc. Pet. Geol.) Bull. 80, 486–504.
Marchand, A.M.E., Haszeldine, R.S., Macaulay, C.I., et al., 2000. Quartz cementation inhibited by crestal oil charge: miller deep water sandstone, UK North Sea. Clay Miner. 35 (1), 201–210.
Marchand, A.M.E., Haszeldine, R.S., Smalley, P.C., et al., 2001. Evidence for reduced quartz-cementation rates in oil-filled sandstones. Geology 29, 915–918.
Marchand, A.M.E., Smalley, P.C., Haszeldine, R.S., et al., 2002. Note on the importance of hydrocarbon fill for reservoir quality prediction in sandstones. AAPG (Am. Assoc. Pet. Geol.) Bull. 86, 1561–1571.
Moore, D.M., Reynolds, R.C., 1997. X-Ray Diffraction and the Identification and Analysis of Clay Minerals. Oxford University Press, New York, p. 378.
Paxton, S.T., Szabo, J.O., Ajdukiewicz, J.M., Klimentidis, R.E., 2002. Construction of an intergranular volume compaction curve for evaluating and predicting compaction and porosity loss in rigid-grain sandstone reservoirs. AAPG (Am. Assoc. Pet. Geol.) Bull. 86 (12), 2047–2067.
Pittman, E.D., Larese, R.E., Heald, M.T., 1992. Clay coats: occurrence and relevance to preservation of porosity in sandstones. In: Houseknecht, D.W., Pittman, E.D. (Eds.), Origin, Diagenesis and Petrophysics of Clay Minerals in Sandstones, vol. 47. SEPM Special Publication, pp. 241–255.
Pittman, E.D., Lumsden, D.N., 1968. Relationship between chlorite coatings on quartz grains and porosity, Spiro Sand, Oklahoma. J. Sediment. Res. 38 (2), 668–670.
Ramm, M., Bjørlykke, K., 1994. Porosity/depth trends in reservoir sandstones: assessing the quantitative effects of varying pore-pressure, temperature history and mineralogy, Norwegian shelf data. Clay Miner. 29 (4), 475–490.
Ren, Z.L., 1996. Research on the relations between geothermal history and oil-gas accumulation in the Ordos Basin. Acta Pet. Sin. 17, 17–24 (in Chinese with English abstract).
Ren, Z.L., Liu, L., Cui, J.P., 2008. Application of tectonic thermal evolution history to hydrocarbon accumulation timing in sedimentary basins. Oil Gas Geol. 29, 503–506 (in Chinese with English abstract).
Ren, Z.L., Zhang, S., Gao, S.L., et al., 2007. Tectonic thermal history and its significance on the formation of oil and gas accumulation and mineral deposit in Ordos Basin. Sci. China Earth Sci. 50, 27–38.
Scherer, M., 1987. Parameters influencing porosity in sandstones: a model for sandstone porosity prediction. AAPG (Am. Assoc. Pet. Geol.) Bull. 71 (5), 485–491.
Shanmugam, G., Moiola, R.J., 1995. Reinterpretation of depositional processes in a classic flysch sequence (pennsylvanian jackfork group), ouachita mountains, Arkansas and Oklahoma. AAPG (Am. Assoc. Pet. Geol.) Bull. 79, 672–695.
Shanmugam, G., 1997. The Bouma sequence and the turbidite mind set. Earth Sci. Rev. 42, 201–229.
Shi, B.H., Zhang, Y., Zhang, L., Yang, Y.J., Li, H., 2012. Hydrocarbon accumulation dating by fluid inclusion characteristics in Chang7 tight sandstone reservoirs of Yanchang Formation in Ordos Basin. Petrol. Geol. 34, 599–603 (in Chinese with English abstract).
Sullivan, K.B., McBride, E.F., 1991. Diagenesis of sandstones at shale contacts and diagenetic heterogeneity, frio formation, Texas (1). AAPG (Am. Assoc. Pet. Geol.) Bull. 75, 121–138.
Sun, N.L., Zhong, J.H., Hao, B., Ge, Y.Z., Swennen, R., 2020. Sedimentological and diagenetic control on the reservoir quality of deep-lacustrine sedimentary gravity flow sand reservoirs of the Upper Triassic Yanchang Formation in Southern Ordos Basin, China. Mar. Petrol. Geol. 112, 104050.
Sun, Z.X., Sun, Z.L., Lu, H.J., Yin, X.J., 2010. Characteristics of carbonate cements in sands tone reservoirs: a case from Yanchang Formation, middle and southern Ordos Basin, China. Petrol. Explor. Dev. 37, 543–551 (in Chinese with English abstract).
Talling, P.J., 2013. Hybrid submarine flows comprising turbidity current and cohesive debris flow: deposits, theoretical and experimental analyses, and generalized models. Geosphere 9, 460–488.
Taylor, T.R., Giles, M.R., Hathon, L.A., Diggs, T.N., Braunsdorf, N.R., Birbiglia, G.V., Kittridge, M.G., Macaulay, C.I., Espejo, I.S., 2010. Sandstone diagenesis and reservoir quality prediction: models, myths, and reality. AAPG (Am. Assoc. Pet. Geol.) Bull. 94, 1093–1132.
Wang, Q., Zhuo, X.Z., Chen, G.J., Li, X.Y., 2007. Characteristics of carbon and oxygen isotopic compositions of carbonate cements in Triassic Yanchang sandstone in Ordos Basin. Nat. Gas. Ind. 27, 28–32 (in Chinese with English abstract).
Worden, R.H., Griffiths, J., Wooldridge, L.J., et al., 2020. Chlorite in sandstones. Earth Sci. Rev. 204, 103105.
Worden, R.H., Mohammed, B., Philip, S., 2018. The effect of oil emplacement on quartz cementation in a deeply buried sandstone reservoir. AAPG (Am. Assoc. Pet. Geol.) Bull. 102 (1), 49–75.
Worden, R.H., Oxtoby, N.H., Smalley, P.C., 1998. Can oil emplacement prevent quartz cementation in sandstones? Petrol. Geosci. 4 (2), 129–137.
Worden, R.H., Morad, S., 2000. Quartz cementation in sandstones: a review of the eyontroversies. In: Worden, R.H. (Ed.), Quartz Cementation in Sandstones. Special Publication of the International Association of Sedimentologists, Oxford, pp. 1–20. Blackwells.
Xu, Q., Shi, W., Xie, X., Manger, W., Mcguire, P., Zhang, X., Wang, R., Xu, Z., 2016. Deep lacustrine sandy debrites and turbidites in the lower Triassic Yanchang Formation, southeast Ordos Basin, central China: facies distribution and reservoir quality. Mar. Petrol. Geol. 77, 1095–1107.
Yang, H., Zhang, W.Z., 2005. Leading effect of the seventh member high-quality source rock of Yanchang Formation in Ordos Basin during the enrichment of low-penetrating oil-gas accumulation: geology and geochemistry. Geochimica 34, 147–154 (in Chinese with English abstract).
Yang, R.C., He, Z.L., Qiu, G.Q., Jin, Z.J., Sun, D.S., Jin, X.H., 2014. A late Triassic gravity flow depositional system in the southern Ordos Basin. Petrol. Explor. Dev. 41, 724–733.
Yang, R., Fan, A., Han, Z., et al., 2017. Lithofacies and origin of the late triassic muddy gravity-flow deposits in the Ordos Basin, central China. Mar. Petrol. Geol. 85, 194–219.
Yang, Y., Li, W., Ma, L., 2005. Tectonic and stratigraphic controls of hydrocarbon systems in the Ordos basin: a multicycle cratonic basin in central China. AAPG (Am. Assoc. Pet. Geol.) Bull. 89 (2), 255–269.
Yao, S.P., Zhang, K., Hu, W.X., Fang, H.F., Jiao, K., 2009. Sedimentary organic facies of the triassic Yanchang Formation in the Ordos Basin. Oil Gas Geol. 30, 74–84 (in Chinese with English abstract).
Zhang, X., Lin, C.M., Cai, Y.F., Qu, C.W., Chen, Z.Y., 2012. Pore-lining chlorite cements in lacustrine-deltaic sandstones from the upper triassic Yanchang Formation, Ordos Basin, China. J. Petrol. Geol. 35, 273–290.
Zhang, X., Lin, C.M., Chen, Z.Y., 2011. Characteristics of chlorite minerals from upper triassic Yanchang Formation in the zhenjing area, Ordos Basin. Acta Geol. Sin. 85, 1659–1671 (in Chinese with English abstract).
Zou, C.N., Zhang, X.Y., Luo, P., et al., 2010. Shallow-lacustrine sand-rich deltaic depositional cycles and sequence stratigraphy of the upper triassic Yanchang Formation, Ordos Basin, China. Basin Res. 22 (1), 108–125.
Zou, C.N., Wang, L., Li, Y., Tao, S.Z., Hou, L.H., 2012. Deep-lacustrine transformation of sandy debrites into turbidites, Upper Triassic, Central China. Sediment. Geol. 265–266, 143–155.
Zhu, S., Wang, X., Qin, Y., et al., 2017. Occurrence and origin of pore-lining chlorite and its effectiveness on preserving porosity in sandstone of the middle Yanchang Formation in the southwest Ordos Basin. Appl. Clay Sci. 148, 25–38.